1989ApJ...340..162M

THE ASTROPHYSICAL JOURNAL, 340:162–180, 1989 May 1
© 1989. The American Astronomical Society. All rights reserved. Printed in U.S.A.

THE RADIATIVE DECELERATION OF ULTRARELATIVISTIC JETS IN ACTIVE GALACTIC NUCLEI

FULVIO MELIA[1]
Department of Physics and Astronomy, Northwestern University
AND
ARIEH KÖNIGL[1]
Department of Astronomy and Astrophysics and Enrico Fermi Institute, University of Chicago
Received 1988 July 14; accepted 1988 October 17

ABSTRACT

We report on detailed calculations of the Compton-scattering interaction between an ultrarelativistic jet that emanates from the vicinity of a massive black hole and the thermal radiation field produced by a surrounding accretion disk. We consider both thin- and thick-disk geometries and model the disk spectrum as a sum of blackbodies, taking into account the intensity enhancement due to internal reflections in disks with central accretion funnels. We compute the Compton-drag deceleration of an initially hyperrelativistic jet for a variety of disk and outflow parameters. The resulting beamed spectrum of the upscattered disk photons is derived self-consistently by a Monte Carlo technique.

Our calculations confirm Phinney's suggestion that the thermal radiation field produced by accretion in an active galactic nucleus could be very effective in decelerating ultrarelativistic jets that are accelerated by electromagnetic or hydromagnetic forces closer to the central black hole. We find that terminal Lorentz factors that are consistent with the values ($\gamma_\infty \lesssim 10$) inferred in superluminal radio sources are readily produced in this model for plausible disk and jet parameters without having to invoke additional acceleration in the interaction zone. It is noted that BL Lac objects and other blazar sources may correspond to relativistic jets that have been decelerated by radiation in a limited luminosity range, with jets associated with brighter (fainter) disks remaining unobserved because they are too weakly (strongly) beamed. We also discuss the kinematic consequences of the transverse gradient in γ_∞ that is predicted by our results.

On the basis of these calculations, we propose a new interpretation of the hard X-ray component that is often detected in the spectra of BL Lac objects. We suggest that this emission be identified with the inverse Compton radiation that is produced in the course of the initial deceleration of the relativistic jets associated with these sources. We demonstrate that the observed properties of the hard X-ray component as well as the inferred values of γ_∞ can be reproduced with this model without violating the constraint that the isotropic flux from the disk should remain lower than the beamed synchrotron flux from the jet. This model also accounts for the strong variability and the frequent occurrence of flat X-ray spectra among the most X-ray–bright BL Lac objects and leads to specific predictions for the cutoff energy of the high-energy emission in these sources.

Subject headings: black holes — BL Lacertae objects — galaxies: jets — galaxies: nuclei — galaxies: X-rays — radiation mechanisms

I. INTRODUCTION

The dynamics of relativistic jets that emanate from active galactic nuclei (AGNs) could be significantly influenced by their Compton-scattering interaction with the ambient radiation field. This effect was first discussed in the context of models for jet production in the funnels of thick radiation-pressure–supported accretion disks. It was noted (Abramowicz and Piran 1980; Sikora and Wilson 1981) that radiatively accelerated particles in an optically thin funnel could not attain highly relativistic speeds because of the Compton drag force, which increases with the particle Lorentz factor γ. Rees (1984) subsequently pointed out that, even if the jet were initially accelerated to a large γ by some nonradiative (e.g., hydromagnetic) mechanism, its terminal speed would still be severely limited by the interaction with the isotropic component of the radiation field in a realistic quasar environment, particularly if it were composed primarily of electron-positron pairs. More recently, Phinney (1987) suggested that the Compton drag exerted by the thermal photons from an accretion disk in the immediate vicinity of the central black hole could be the main reason why the jet Lorentz factors that are inferred from the apparent superluminal motions measured in compact radio sources typically do not exceed $\sim 10 h_0^{-1}$ (where $h_0 \equiv H_0/100$ km s^{-1} Mpc^{-1}). The constraint imposed by the disk radiation field is particularly relevant in view of the fact that, in certain electromagnetic acceleration schemes (e.g., Michel 1987), the jets could attain hyperrelativistic speeds (Lorentz factors as high as 10^{10}) close to the central source.

The interaction of a relativistic jet with the ambient radiation field could also have important spectral consequences. Begelman and Sikora (1987) have calculated the Compton upscattering of the nonthermal AGN background radiation by a relativistic outflow and demonstrated that it leads to a highly polarized, Doppler-boosted emission. They suggested that the upscattered nonthermal

[1] Presidential Young Investigator.

© American Astronomical Society • Provided by the NASA Astrophysics Data System

1989ApJ...340..162M

flux could contribute significantly to the near-IR–X-ray spectra of sources that are observed at a small angle to the jet direction. However, the measured infrared through soft X-ray emission in these sources is probably dominated by the beamed synchrotron radiation from the jet itself (e.g., Königl 1981), which in any case must be invoked to account for the flat radio spectra observed in such radio-loud blazars (e.g., Maraschi *et al.* 1986). Furthermore, since the bolometric luminosity in "unbeamed" quasars is generally dominated by the optical/UV/soft X-ray "big bump" (e.g., Malkan and Sargent 1982; Elvis *et al.* 1986), it is clearly important to include this emission component in the calculation of the upscattered spectrum. In fact, since the "big bump" likely represents the thermal emission from the nuclear accretion disk (e.g., Shields 1978), it probably also dominates the ambient radiation field in the jet deceleration zone. The detailed spectral distribution of the upscattered "big bump" photons may thus be expected to provide important clues to the physical conditions near the central black hole.

In this paper, we carry out a detailed study of the dynamical interaction between a highly relativistic jet and the thermal radiation field from an AGN accretion disk, and determine self-consistently the Comptonized spectrum arising from this interaction. In § II we present a simple model that is meant to capture the essential radiative and geometrical features of realistic disk configurations, and we describe the calculation of the disk radiation field, the Compton-drag interaction with the jet, and the emitted spectrum. The results of these calculations for several representative disk and jet parameters are given in § III. In § IV we discuss the astrophysical implications of these results. We consider the effects of the jet-radiation interaction on the kinematic properties of relativistic outflows and on their emission spectra. We point out, in particular, that this scenario provides a natural explanation for the highly variable hard X-ray component that has been detected in several BL Lac objects. Our conclusions are summarized in § V.

II. CALCULATIONAL PROCEDURE

a) The Accretion Disk

An attractive explanation for the strong optical/UV/soft X-ray excess in certain quasars (e.g., PG 1211+143; Bechtold *et al.* 1987) is the release of gravitational energy through an accretion disk with characteristic (maximum) temperature $T_{\max} \lesssim 10^5$ K, with opacity, inclination, and reflection effects taken into account (Czerny and Elvis 1987; Madau 1988; Wandel and Petrosian 1988). In order to bring out the dependence of our results on the essential features of the accretion disk, we have modeled its emission as a simple sum of blackbodies. In this basic model, the temperature distribution as a function of equatorial radius R is given by

$$T(R) = T_{\max}\left\{7\left(\frac{49}{36}\frac{R_{\rm in}}{R}\right)^3\left[1-\left(\frac{R_{\rm in}}{R}\right)^{1/2}\right]\right\}^{1/4} . \tag{1}$$

The maximum temperature $T_{\max} = (3GM\dot{M}/56\pi\sigma R_{\max}^3)^{1/4}$ (where M is the black hole mass, $\dot{M}$ is the mass accretion rate, G is the gravitational constant, and σ is the Stefan-Boltzmann constant) is attained at the (equatorial) radius $R_{\max} = (49/36)R_{\rm in}$, where $R_{\rm in} = \eta R_g$ ($R_g \equiv GM/c^2$) is the innermost disk radius and $\eta \approx 2$–10.

The accretion disk is unlikely to remain thin at the super-Eddington luminosities inferred for many of the sources with an optical/UV/soft X-ray excess. In particular, the disk may develop a funnel, within which reflection effects increase the radiation energy density relative to the net flux (Sikora 1981). In our simple generalization from a thin disk, we "fold" the disk with an angle θ_f to the normal at $R_{\rm in}$ and then "fold" it back into a flat disk at R_f (Fig. 1). This configuration is, therefore, completely specified by the parameters $R_{\rm in}$, R_f, θ_f, and $T_{\max}$.

Strictly speaking, the temperature distribution given by equation (1) is valid only for a thin disk ($\theta_f \approx \pi/2$). However, we expect the energy dissipation rate in a centrally condensed disk to be only weakly dependent on θ_f when M and $\dot{M}$ are held constant. We therefore assume that the flux radiated per unit area projected onto the equatorial plane is independent of θ_f and take $T(R)$ to be the effective temperature of this projected emission surface.

Within the funnel, balance of forces in the direction normal ($\boldsymbol{n}$) to the surface is achieved when $F_e - F^n_{\rm abs} = \sigma T(R)^4$, where $F^n_{\rm abs}$ is the normal component of the absorbed flux and F_e is the sum of the locally generated flux and the (isotropically) reemitted flux. Dividing the disk into a finite number of rings N, we write for the kth ring

$$(F_e)_k - \sum_l B^l_k (F_e)_l \approx \sigma T(R_k)^4 , \tag{2}$$

where

$$B^l_k = \frac{1}{\pi}\int_{\Omega_{kl}}\left(\frac{\nu_{\rm abs}}{\nu_{\rm em}}\right)^4 \boldsymbol{n}\cdot d\boldsymbol{\Omega} , \tag{3}$$

$\nu_{\rm em}$ and $\nu_{\rm abs}$ are the emitted and absorbed radiation frequencies, respectively, and Ω_{kl} is the solid angle subtended by the lth ring at the kth ring (Sikora 1981).

If we ignore the gravitational redshift,

$$B^l_k \approx \frac{1}{\pi}\int_{\Omega_{kl}} \boldsymbol{n}\cdot d\boldsymbol{\Omega} . \tag{4}$$

Because of photon trapping inside the event horizon, we ignore the contribution to $F^n_{\rm abs}$ from the opposite funnel. With our simplified geometry, the integral (4) can be evaluated directly to give

$$B^l_k = \frac{5}{2}(\cos^2\theta_f \sin^4\theta_f) R_l^2 R_k \Delta \frac{F(2, 1/2; 4; X)}{(R_k^2 + R_l^2 - 2R_k R_l \cos 2\theta_f)^2} , \tag{5}$$

© American Astronomical Society • Provided by the NASA Astrophysics Data System

1989ApJ...340..162M

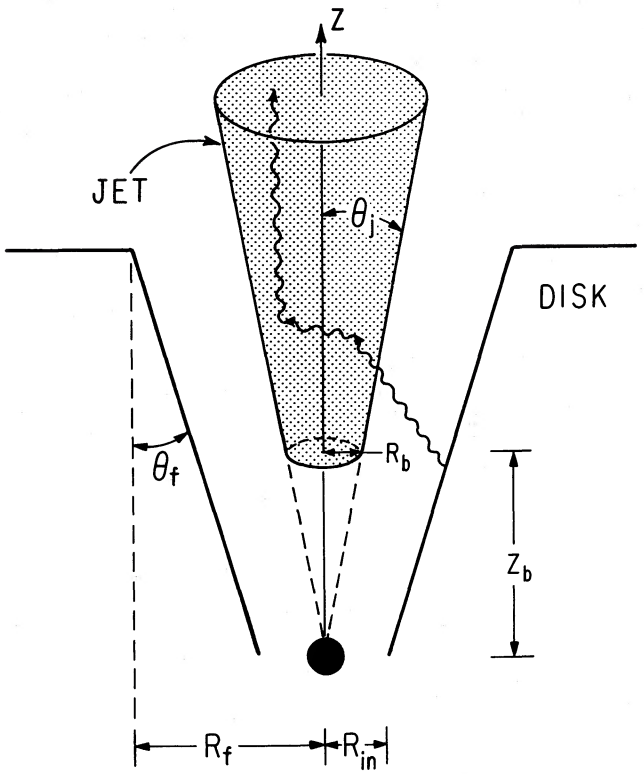


FIG. 1.—Geometrical features of the simple disk and jet configuration used in our model. The accretion disk is specified by its inner (equatorial) radius R_{in}, the outer radius R_f of the central funnel, and the funnel half-opening angle θ_f. The jet is described by the radius R_b and height z_b of its base as well as by its half-opening angle θ_j.

where

$$X \equiv \frac{4R_k R_l \sin^2 \theta_f}{R_k^2 + R_l^2 - 2R_k R_l \cos 2\theta_f} . \tag{6}$$

Here R_i is the radius of the ith ring, Δ is the width of each ring along the surface of the disk, and F is Gauss's hypergeometric function. Since $X \leq 1$, we use

$$F = \begin{cases} 8/5 & \text{when } X = 1 , \\ \sum_{n=0}^{\infty} a_n X^n & \text{when } X < 1 , \end{cases} \tag{7}$$

where

$$a_{n+1} = \frac{(n+2)(2n+1)}{(n+4)(2n+2)} a_n , \tag{8}$$

with $a_0 = 1$.

b) The Compton-Drag Interaction

As noted in § I, the motion of particles in a relativistic jet is constrained by the drag of the photons from the nuclear accretion disk. The jet is rapidly decelerated or accelerated, depending on whether the Lorentz factor γ is greater than or smaller than some critical value, which is a function of the physical parameters of the disk and the jet (Phinney 1987). The particles in a cold electron-positron ($e^- e^+$) or electron-proton ($e^- p$) jet gain or lose energy $p^0 = \gamma mc^2$ according to

$$c\beta \frac{dp^0}{dr} = -\int d\nu\, \sigma(\gamma, \nu) \left[\gamma^2 \int I_\nu(\theta, \phi)(1 - \beta \cos \theta)^2 \, d\Omega - \int I_\nu(\theta, \phi)(1 - \beta \cos \theta) \, d\Omega \right] \tag{9}$$

(O'Dell 1981; Phinney 1982), where $I_\nu(\theta, \phi)$ is the specific intensity of radiation in a direction (θ, ϕ) with respect to the electron (or positron) direction of motion, and $\sigma(\gamma, \nu)$ is the total scattering cross section. In writing this expression, we have ignored the effects of multiple scatterings on the dynamics, since these are not energetically important. The optical depth for scattering is proportional to $(1 - \boldsymbol{k} \cdot \boldsymbol{\beta})$, where $\boldsymbol{k}$ and $\boldsymbol{\beta}$ are the photon direction and electron velocity (in units of the speed of light c), respectively. Since the singly scattered photons are highly beamed along the jet, this factor is of order γ^{-2} for higher order scatterings (Begelman and Sikora

© American Astronomical Society • Provided by the NASA Astrophysics Data System

1989ApJ...340..162M

1987). However, multiple scatterings could be important in determining the emitted spectrum, and we therefore include them in our spectral calculations.

The particle discharge in the jet may change with radius as a result of several pair production processes: (1) $e^{\pm} + \gamma \rightarrow e^{\pm} + e^{+} + e^{-}$, for which the threshold photon energy in the jet rest frame is $\epsilon_0' = 4m_e c^2$; (2) $p + \gamma \rightarrow p + e^{+} + e^{-}$, for which $\epsilon_0' = 2m_e c^2$; and (3) $\gamma + \gamma \rightarrow e^{+} + e^{-}$, in which an upscattered γ-ray collides with a low-energy photon. Since the upscattered γ-ray has an energy $< \gamma m_e c^2$ in the observer's frame, the soft-photon energy threshold for reaction 3 is $\epsilon_0 \gtrsim 2m_e c^2/\gamma$. (High-energy γ-rays can also arise from the decay of pions that are produced in the reaction $p + \gamma \rightarrow p + \pi^0$, for which the threshold photon energy is $\epsilon_0' \approx 264 m_e c^2$.) In our calculations, the thermal emission from the disk is characterized by a temperature $T_{\max} \approx 10^5$ K, corresponding to photon energies $\epsilon_0 \lesssim 3k_B T_{\max} \approx 5 \times 10^{-5} m_e c^2$ (where k_B is the Boltzmann constant), so $\epsilon_0' \lesssim 2\gamma\epsilon_0 \lesssim 10^{-4}\gamma m_e c^2$. Compositional changes in the jet may, therefore, be ignored as long as $\gamma \lesssim 10^4$. Since this condition is sufficient to guarantee that $\epsilon_0' \lesssim m_e c^2$, we may also ignore recoil effects. Thus, putting $\sigma(\gamma, \nu) = \sigma_T$, and assuming uniform composition, we reduce equation (9) to

$$\frac{d\gamma}{dr} = -\left(\frac{\sigma_T}{mc^3}\right)\left[\gamma\sqrt{\gamma^2 - 1}\int I(1 + \cos^2\theta)\, d\Omega + (1 - 2\gamma^2)\int I\cos\theta\, d\Omega\right], \tag{10}$$

where $I = \int dv I_v(\theta, \phi)$ and $m = m_e$ or m_p for $e^- e^+$ and $e^- p$ jets, respectively.

We write the integrals in equation (10) as sums over the N rings, so that at the coordinates (r, θ_0) along a particle trajectory,

$$\frac{d\gamma}{dr} = -\left(\frac{\sigma_T}{mc^3}\right)\left(\frac{\gamma^3\Upsilon_1}{\sqrt{\gamma^2 - 1}} - \Upsilon_2\right), \tag{11}$$

with

$$\Upsilon_1 = \Delta\sum_{l=1}^{N} I_l R_l J_{1l}, \tag{12}$$

$$\Upsilon_2 = \Delta\sum_{l=1}^{N} I_l R_l J_{2l}, \tag{13}$$

where $I_l = (F_e)_l/\pi$ and R_l are, respectively, the intensity and radius of the lth ring. The integrals J_{1l} and J_{2l} are

$$J_{1l} = \int_0^{2\pi} d\eta \sin^2\theta_1 \frac{\boldsymbol{n}\cdot\boldsymbol{\beta}}{b^2}\left(1 - \frac{\sqrt{\gamma^2 - 1}}{\gamma}\cos\theta\right)^2, \tag{14}$$

and

$$J_{2l} = \int_0^{2\pi} d\eta \sin^2\theta_1 \frac{\boldsymbol{n}\cdot\boldsymbol{\beta}}{b^2}\left(\frac{\gamma}{\sqrt{\gamma^2 - 1}} - \cos\theta\right), \tag{15}$$

where

$$\cos\theta = -\sin\theta_0 \sin\theta_1 \cos\phi_1 + \cos\theta_0 \cos\theta_1, \tag{16}$$

$$\boldsymbol{n}\cdot\boldsymbol{\beta} = \begin{cases} \cos\theta_f \sin\theta_1 (\cos\eta \cos\phi_1 + \sin\eta \sin\phi_1) + \sin\theta_f \cos\theta_1, & R_l < R_f \\ \cos\theta_1, & R_l \geq R_f \end{cases} \tag{17}$$

with

$$\theta_1 \equiv \tan^{-1}(b/c), \tag{18}$$

$$\phi_1 \equiv \cos^{-1}\left[\left(\frac{R_l}{b}\right)\cos\eta - \left(\frac{a}{b}\right)\right], \tag{19}$$

and $a \equiv r \sin\theta_0$, $b \equiv (a^2 + R_l^2 - 2aR_l\cos\eta)^{1/2}$, and $c \equiv r\cos\theta_0 - (R_l - R_{in})/\tan\theta_f$.

c) *The Emitted Spectrum*

We use a Monte Carlo simulation to determine the Comptonized spectrum arising from the interaction between the thermal photons from the disk and the particles in the ultrarelativistic jet. We allow for the variation of γ along different particle trajectories by integrating equation (11) and storing the values in a two-dimensional array corresponding to the (r, θ_0)-plane. The spectrum is calculated by means of a random-walk model for the spatial transport, taking into account (1) the appropriate randomization of initial photon energy and photon mean free path (including light travel-time effects) as well as (2) the angular dependence of the Klein-Nishina differential cross section and scattering in a three-dimensional geometry.

The particle number density (assumed to be uniform across the jet) can be written as

$$n = \frac{\tau_\perp}{2R_b\sigma_T}\left(\frac{r}{z_b/\cos\theta_0}\right)^{\delta}$$
$$\approx 1 \times 10^{10}\left(\frac{R_b}{5R_g}\right)^{-1}\left(\frac{M}{10^8 M_\odot}\right)^{-1}\left(\frac{\tau_\perp}{1}\right)\left(\frac{r}{z_b/\cos\theta_0}\right)^{\delta} \text{cm}^{-3}, \tag{20}$$

© American Astronomical Society • Provided by the NASA Astrophysics Data System

1989ApJ...340..162M

where $\tau_\perp$ is the Thomson optical depth perpendicular to the jet axis at the base z_b, and R_b is the jet radius at z_b. (Here z_b may represent the length of the jet acceleration zone or the extent of the region where $\tau_\perp > 1$ so that radiative deceleration is ineffective; see the discussion of e^-e^+ jets in § III*b*.) The index δ specifies the two jet geometries we consider here: (1) parallel jets with $\delta = 0$ and (2) fan jets with $\delta = -2$. For fan jets, the jet half-opening angle θ_j is fixed by R_b and z_b (see Fig. 1).

We follow the photons until they leave the jet, and then record their energy and inclination angle with respect to the jet axis. Since the Comptonized photons are typically boosted into a cone of half-opening angle $\sim 1/\gamma$, where γ is the jet Lorentz factor at the point of last scattering, effects due to reflection in the disk can be ignored unless the funnel is extremely steep (i.e., sin $\theta_f \lesssim 1/\gamma_\infty$, where γ_∞ is the terminal jet Lorentz factor). Any Comptonized photons that penetrate the disk are effectively lost from the observed spectrum because of the low γ-ray albedo (~ 0.2–0.3) at these energies (e.g., Melia, Rappaport, and Joss 1986).

The Comptonized flux is normalized by direct comparison of the number of upscattered photons to the number of photons emitted by the disk. The disk flux density viewed near the jet axis is

$$F^D(\epsilon_i, r) \approx \frac{n_\gamma^D(\epsilon_i)\epsilon_i}{(\Delta\epsilon)\Lambda}\frac{2L_{\rm disk}}{4\pi r^2}, \tag{21}$$

where

$$L_{\rm disk} = \frac{1}{2}\frac{GM\dot{M}}{R_{\rm in}}, \tag{22}$$

$$\Lambda = \sum_j n_\gamma^D(\epsilon_j)\epsilon_j, \tag{23}$$

with $\Delta\epsilon$ the width of the energy channels ϵ_i and $n_\gamma^D(\epsilon_i)$ the number of disk photons emitted within the interval $\Delta\epsilon$ at energy ϵ_i. The corresponding Comptonized flux density is

$$F^J(\epsilon_i, r, \theta) \approx \frac{n_\gamma^J(\epsilon_i, \theta)\epsilon_i}{(\Delta\epsilon)\Lambda}\frac{L_{\rm disk}}{2A_\theta(r)}, \tag{24}$$

where $A_\theta(r)$ is the cross-sectional area of the beamed emission and $n_\gamma^J(\epsilon_i, \theta)$ is the number of photons scattered into an angular annulus $\Delta\theta$ in the direction θ and within the energy interval $\Delta\epsilon$ at ϵ_i. In the case of a parallel jet ($\delta = 0$), $A_\theta(r) \approx 2\pi r^2\theta\,\Delta\theta$, so

$$\frac{F^J(\epsilon_i, \theta)}{F^D(\epsilon_i)} \approx \frac{1}{2\theta\,\Delta\theta}\frac{n_\gamma^J(\epsilon_i, \theta)}{n_\gamma^D(\epsilon_i)}. \tag{25}$$

Although our model has several free parameters ($T_{\rm max}$, $R_{\rm in}$, R_f, θ_f, z_b, R_b, γ_i, $\tau_\perp$, and δ, which determine γ_∞), at least four of these are constrained by the observations: (1) The terminal Lorentz factor γ_∞ is inferred from the superluminal motion associated with the extended jets in sources such as BL Lac to be $\lesssim 10$ (e.g., Porcas 1987). (2) The measurement of a soft X-ray excess in a source like PG 1211+143 implies a maximum disk temperature $\lesssim 5 \times 10^5$ K for a sum-of-blackbodies model (Bechtold *et al.* 1987), and an effective peak temperature as low as $\sim 3 \times 10^4$ K if opacity effects are included (Czerny and Elvis 1987). Studies of quasar spectra below the Lyman limit indicate, however, that the peak disk temperature typically lies above this lower bound (Elvis 1988). (3) The fact that this thermal component contributes a flux at most comparable to the synchrotron emission from the extended jet places an upper limit on the effective area of the accretion disk (which scales roughly as the square of the black hole mass). For example, in the source PKS 2155−304 (e.g., Urry and Mushotzky 1982), the apparent absence of a UV/soft X-ray excess implies a black hole mass $M \lesssim 10^8\,M_\odot$. Finally, (4) the observed synchrotron luminosity from a jet may be used to constrain its total kinetic luminosity when an efficiency ε for the conversion of mechanical to synchrotron power is assumed. Specifically, for an observed synchrotron luminosity

$$L_s = \frac{4\pi D^2 F_s(\theta)}{\mathscr{D}^4(\theta)}, \tag{26}$$

where D is the luminosity distance to the source, $F_s(\theta)$ is the frequency-integrated synchrotron flux detected at an inclination angle θ to the jet axis, and $\mathscr{D}(\theta)$ is the Doppler factor, we infer an initial total jet power

$$L_{\rm jet} = \varepsilon^{-1}\left(\frac{\gamma_i}{\gamma_\infty}\right)L_s. \tag{27}$$

For the BL Lac object PKS 2155−304 modeled below (see § III*b*), this gives

$$L_{\rm jet} \approx 3 \times 10^{47}\left(\frac{\varepsilon}{0.01}\right)^{-1}\left(\frac{\gamma_i}{10^3}\right)\left(\frac{\gamma_\infty}{10}\right)^{-5}\left(\frac{F_s}{2 \times 10^{-9}\ {\rm ergs\ cm^{-2}\ s^{-1}}}\right)\left(\frac{D}{1\ {\rm Gpc}}\right)^2\ {\rm ergs\ s^{-1}}, \tag{28}$$

where the viewing angle θ is assumed to correspond to a Doppler-favored inclination, $\theta \approx 1/\gamma_\infty$ and $\mathscr{D} \approx \gamma_\infty$. Since

$$L_{\rm jet} \approx \pi R_b^2 \gamma_i nmc^3, \tag{29}$$

the optical depth at the base of a relativistic jet emanating from this source would be

$$\tau_\perp \approx 0.04\left(\frac{R_b}{5R_g}\right)^{-1}\left(\frac{M}{10^8\ M_\odot}\right)^{-1}\left(\frac{F_s}{2 \times 10^{-9}\ {\rm ergs\ cm^{-2}\ s^{-1}}}\right)\left(\frac{D}{1\ {\rm Gpc}}\right)^2\left(\frac{\gamma_\infty}{10}\right)^{-5}\left(\frac{\varepsilon}{0.01}\right)^{-1}\left(\frac{m}{m_p}\right)^{-1}. \tag{30}$$

Of the remaining parameters, only θ_f, z_b, and γ_i (but not R_f, R_b, or δ) generally have a significant effect on the spectrum (see § III*b*).

© American Astronomical Society • Provided by the NASA Astrophysics Data System

1989ApJ...340..162M

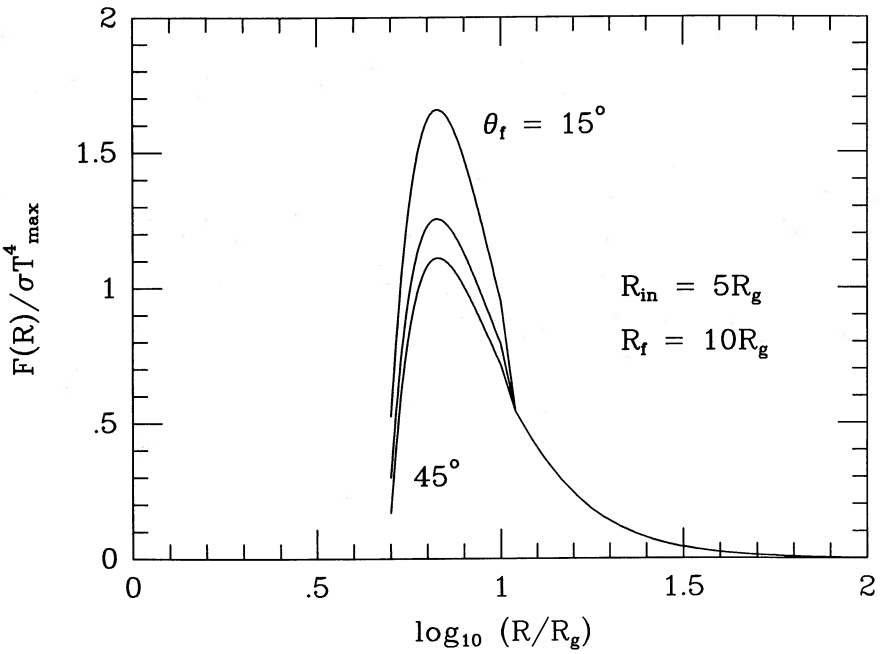


FIG. 2.—Distribution of disk flux F_e for $R_{in} = 5R_g$, $R_f = 10R_g$, and three different funnel half-opening angles θ_f. The enhancement in F_e due to internal reflections within the funnel is particularly strong for the smaller values of θ_f.

III. NUMERICAL RESULTS

a) Jet Dynamics

The rate at which the particles in a cold jet gain or lose energy is roughly proportional to the intensity of the intercepted disk radiation (see eq. [10]). The intensity along the jet varies with the funnel half-opening angle θ_f because of the amplification effect of multiple reflections within the funnel and as a result of its dependence on the solid angle subtended by the emitting surface element in the disk. Figure 2 shows the disk flux $F_e(R)$ for three values of θ_f (15°, 30°, and 45°) in a disk with inner radius $R_{in} = 5R_g$ and outer funnel radius $R_f = 10R_g$. Steeper funnels enhance the flux $F_e(R)$ and so give rise to more rapidly decelerated jets.

The combined effect of the flux enhancement and funnel geometry on the jet deceleration is evident in Figure 3, which shows the distribution of γ along the axis of an e^-p jet for three different values of the funnel half-opening angle. This jet is launched with an

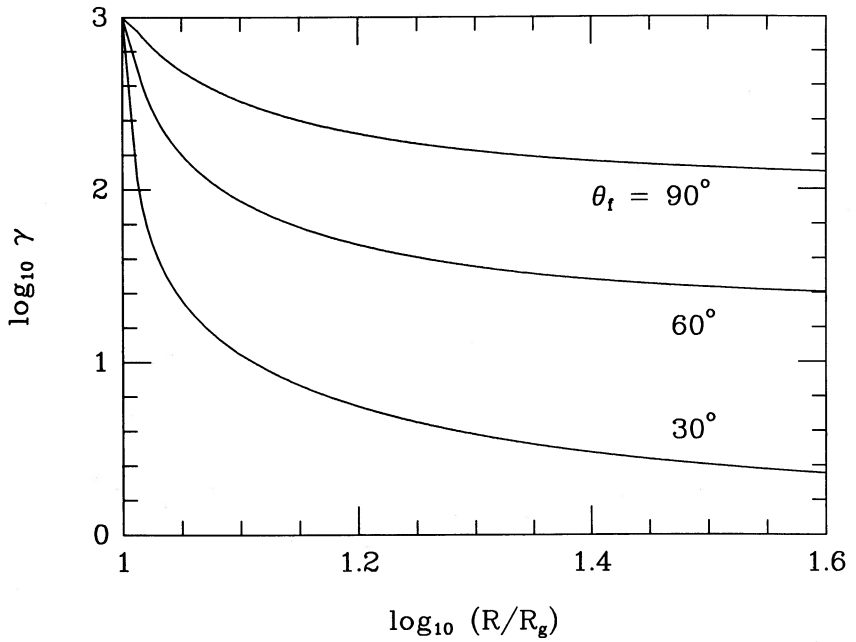


FIG. 3.—Distribution of the Lorentz factor γ along the axis of an e^-p jet that is launched with an initial Lorentz factor $\gamma_i = 10^3$ at $z_b = 10R_g$ (with $M = 10^8\ M_\odot$), for three different funnel half-opening angles. The disk parameters in this case are $R_{in} = 5R_g$, $R_f = 50R_g$, and $T_{max} = 2 \times 10^5$ K. The deceleration is greater for the smaller values of θ_f because of the flux enhancement within the funnel (see Fig. 2).

© American Astronomical Society • Provided by the NASA Astrophysics Data System

1989ApJ...340..162M

initial Lorentz factor $\gamma_i = 10^3$ at a height $z_b = 10R_g$ above a black hole of mass $M = 10^8\ M_\odot$. In this example, the accretion disk is characterized by a maximum temperature $T_{max} = 2 \times 10^5$ K, an inner radius $R_{in} = 5R_g$, and an outer funnel radius $R_f = 50R_g$. The terminal Lorentz factor γ_∞ in the jet drops from ~ 125 for a flat disk ($\theta_f = 90°$) to ~ 2 when $\theta_f = 30°$. The behavior of e^-e^+ jets is qualitatively similar to that of e^-p jets, but their deceleration is always significantly greater because of the much smaller mean mass per particle (see eq. [10]).

To test the dependence of the jet dynamics on the other parameters of our model, we have integrated equation (11) for various values of γ_i, T_{max}, and z_b. The results of these calculations are summarized in Figures 4*a* and 4*b*. The curves in these plots represent the variation of γ_i with T_{max} and z_b when the terminal Lorentz factor γ_∞, chosen to sample the range of values inferred from the apparent superluminal motions in radio sources such as BL Lac, is held fixed. Other than the funnel angle θ_f, the parameters in these calculations are the same as those in Figure 3.

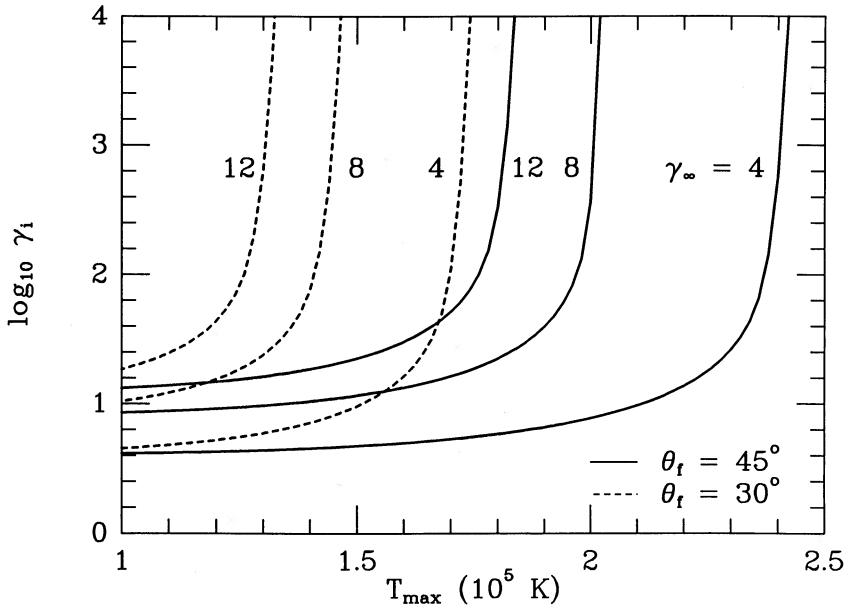


FIG. 4*a*

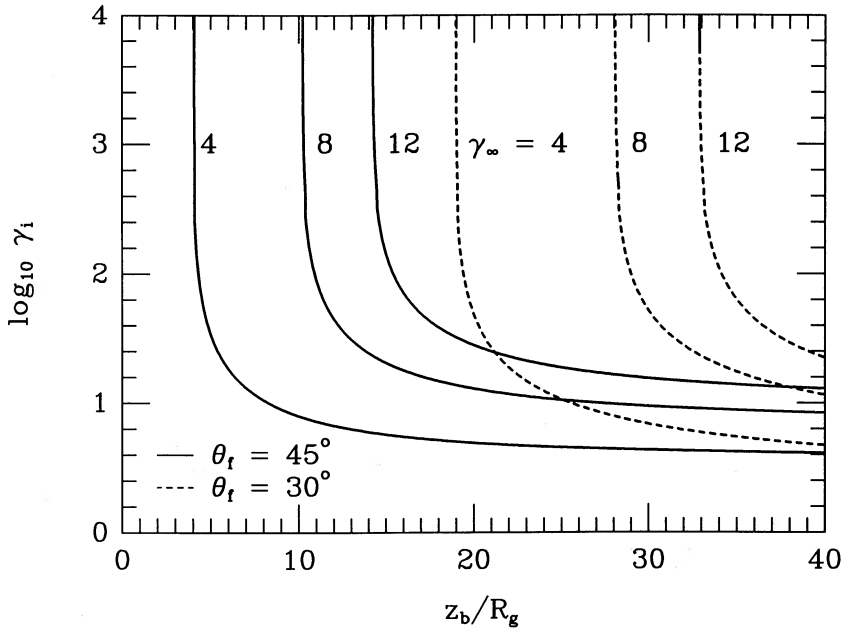


FIG. 4*b*

FIG. 4.—(*a*) Variation of γ_i with T_{max} along the axis of an e^-p jet for constant values of the terminal Lorentz factor γ_∞. The curves correspond to funnels with half-opening angle $\theta_f = 45°$ (*solid*) and $\theta_f = 30°$ (*dashed*). The other parameters are the same as in Fig. 3. (*b*) Variation of γ_i with z_b along the axis of an e^-p jet for constant values of the terminal Lorentz factor γ_∞. The disk parameters are the same as in Fig. 3.

© American Astronomical Society • Provided by the NASA Astrophysics Data System

1989ApJ...340..162M

Figures 4*a* and 4*b* reveal several important features of the Compton-drag effect on the jet dynamics: (1) For each value of the disk temperature T_{max}, there exists a maximum attainable terminal Lorentz factor γ_∞ independent of γ_i. This behavior (manifested in the divergence of γ_i toward high values of T_{max} along trajectories of constant γ_∞) is a consequence of the fact that highly relativistic jets tend to decelerate more rapidly than jets with smaller values of γ_i owing to the strong dependence of the deceleration on the Lorentz factor ($d\gamma/dr \propto \gamma^2$ in the Thomson scattering regime; see § IV*a* for a further discussion of this point). (2) For a fixed T_{max}, γ_∞ drops as the funnel steepens because a narrow funnel can produce the same radiative intensity along the jet as a wider funnel with a higher temperature. (3) For a fixed T_{max}, there exists an upper limit to γ_∞ for any given value of z_b, which again reflects the dependence of the deceleration efficiency on γ_i. Since narrow funnels produce larger radiative intensities (and hence a stronger deceleration) along the jet than wider funnels, z_b must increase as θ_f decreases in order for γ_∞ to remain unchanged.

Another interesting aspect of the Compton-drag deceleration is that it is sensitive to the inclination angle of the jet with respect to the disk (Fig. 5). Because of this effect, which arises from the dependence of the Compton drag force on the scattering angle and on the surface brightness distribution in the disk, a fan-shaped jet with initially uniform γ_i would emerge from the deceleration region with a measurable transverse distribution of Lorentz factors. This process may thus contribute to the collimation of relativistic jets by limiting the high-γ_∞ core of the decelerated outflow to a relatively narrow cone about the jet axis. In the example shown here, γ_∞ ranges from ~ 130 along the axis to ~ 10 at $\theta_{xj} = 80°$. Additional implications of the induced transverse gradient in γ_∞ are discussed in § IV.

b) The Comptonized Spectrum

We calculated the upscattered spectrum arising from the Compton-drag interaction for two different jet compositions ($e^- p$ and $e^- e^+$) and for two different jet geometries characterized by the parameter δ (see eq. [20]). Figures 6, 7, 8, and 9 show illustrative spectra for representative disk and jet parameters. In each case, we have assumed $R_{in} = 5R_g$, $R_f = 50R_g$, and $M = 10^8\, M_\odot$. The total flux was normalized on the basis of equations (26) and (28), setting $\gamma_\infty = 8$, $\varepsilon = 0.01$, and using the parameters of the BL Lac object PKS 2155−304 ($F_s \approx 2 \times 10^{-9}$ ergs cm^{-2} s^{-1}, $D \approx 1$ Gpc; Urry and Mushotzky 1982). Also indicated in these figures are the contributions to the observed spectrum from the disk and the individual multiplicities of scattering.

The spectra produced by parallel ($\delta = 0$) $e^- p$ jets with a base $z_b = 10R_g$, initial Lorentz factor $\gamma_i = 10^3$, and terminal Lorentz factor $\gamma_\infty \approx 8$ are shown in Figures 6*a*–6*d* for different viewing angles with respect to the jet axis. In this example, the jet radius is $R_b = 5R_g$, the maximum disk temperature is $T_{max} = 2 \times 10^5$ K, and the funnel half-opening angle is $\theta_f = 45°$. Two features of these spectra deserve particular attention. The first is the distinct cutoff (ϵ_{max}) at high energy, and the second is the variation of the spectral shape with viewing angle θ. We can understand the behavior of the cutoff by noting that the highest energy photons result from forward scattering, so that $\epsilon_{max} \approx \min(\gamma^2 \epsilon_{0,max}, \gamma m_e c^2)$, where $\epsilon_{0,max}$ is a characteristic photon energy in the Wien portion of the thermal radiation from the disk. Thus, spectral components arising from different parts of the jet are predicted by this model to have different cutoff energies corresponding to the different γ's where the scattering takes place. As we have already seen in Figure 3, hyperrelativistic jets in a thick disk decelerate very rapidly near the base z_b, so the Lorentz factor is very close to its asymptotic value γ_∞ over most of the central funnel. Thus, the upscattered component produced near z_b (where $\gamma \approx \gamma_i$) has the highest cutoff energy, and the cutoff value becomes significantly smaller for radiation emitted farther out along the jet. Now, the upscattered radiation is preferentially beamed in the direction of motion of the scattering particle within a cone of half-opening angle $\sim 1/\gamma$, where γ is the Lorentz factor before the scattering. Hence, for a jet observed near the axis, the cutoff energy would be $\epsilon_{max}(\theta \approx 0) \approx \min(\gamma_i^2 \epsilon_{0,max}$,

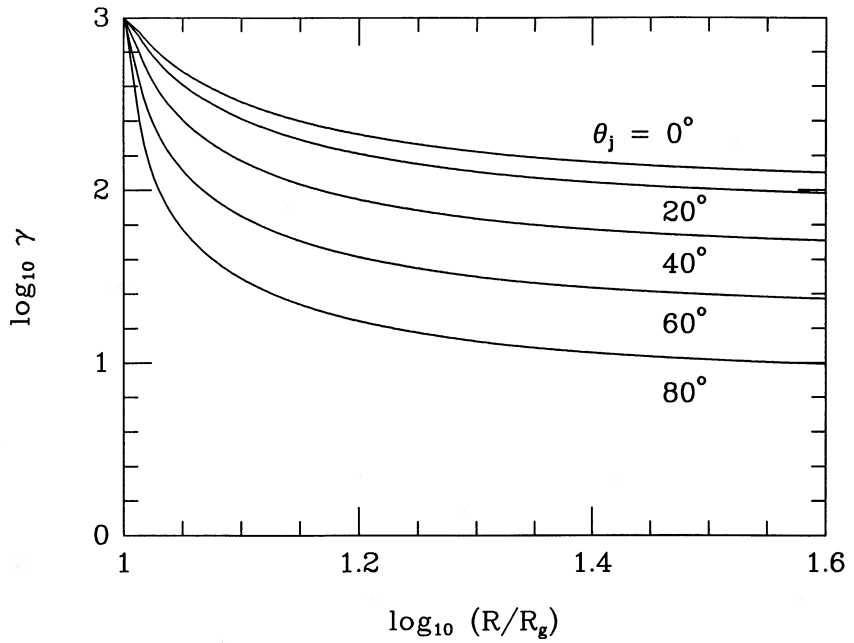


FIG. 5.—Distribution of γ in an $e^- p$ jet along radial trajectories that are inclined at an angle θ_j to the axis, for five different inclinations. The disk parameters are the same as in Fig. 3, with $\theta_f = 90°$.

© American Astronomical Society • Provided by the NASA Astrophysics Data System

1989ApJ...340..162M

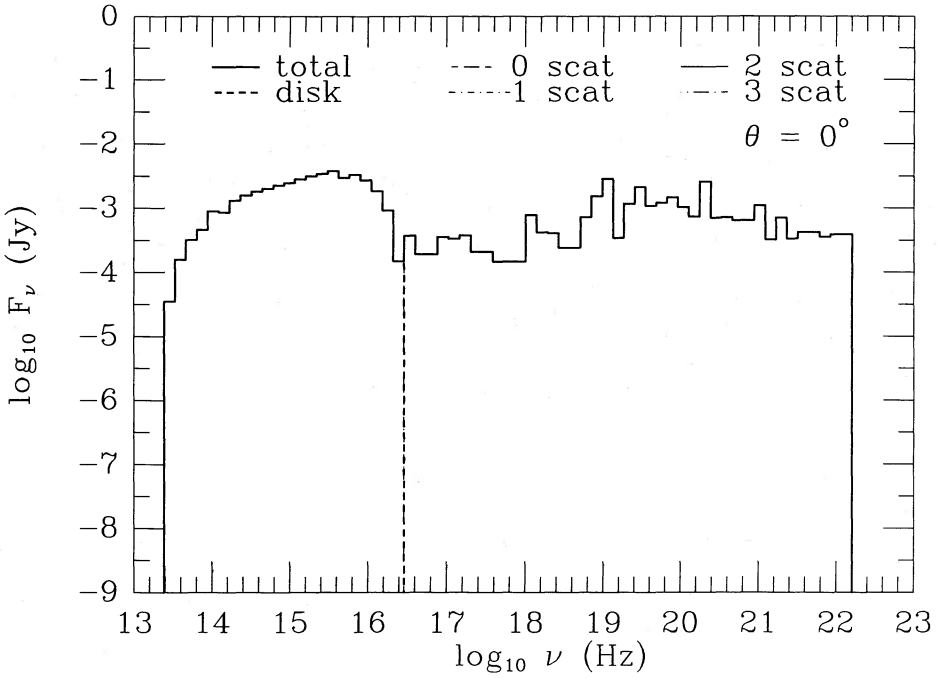


FIG. 6*a*

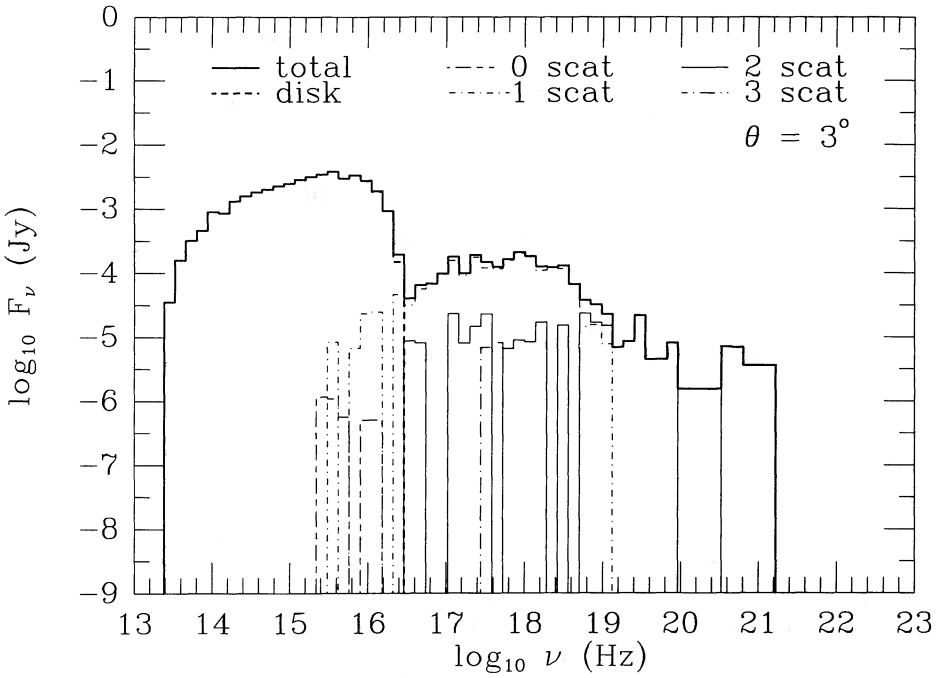


FIG. 6*b*

FIG. 6.—(*a*) Comptonized spectrum arising from the upscattering of (thermal) disk radiation by the particles in a cylindrical ($\delta = 0$) $e^- p$ jet, assuming the disk parameters of Fig. 3, with $\theta_f = 45°$. The initial Lorentz factor is $\gamma_i = 10^3$, the terminal Lorentz factor is $\gamma_\infty \approx 8$, and the radius of the jet is $R_b = 5R_g$. The viewing angle with respect to the jet axis is $\theta = 0°$, and the flux density is normalized using the inferred synchrotron emission of the BL Lac object PKS 2155−304 (see text). Also indicated are the contributions to the total spectrum from the disk and from the individual multiplicities of scattering within the jet. (*b*) Same as (*a*), except that the viewing angle is $\theta = 3°$. (*c*) Same as (*a*), except that the viewing angle is $\theta = 9°$. (*d*) Same as (*a*), except that the viewing angle is $\theta = 19°$.

© American Astronomical Society • Provided by the NASA Astrophysics Data System

1989ApJ...340..162M

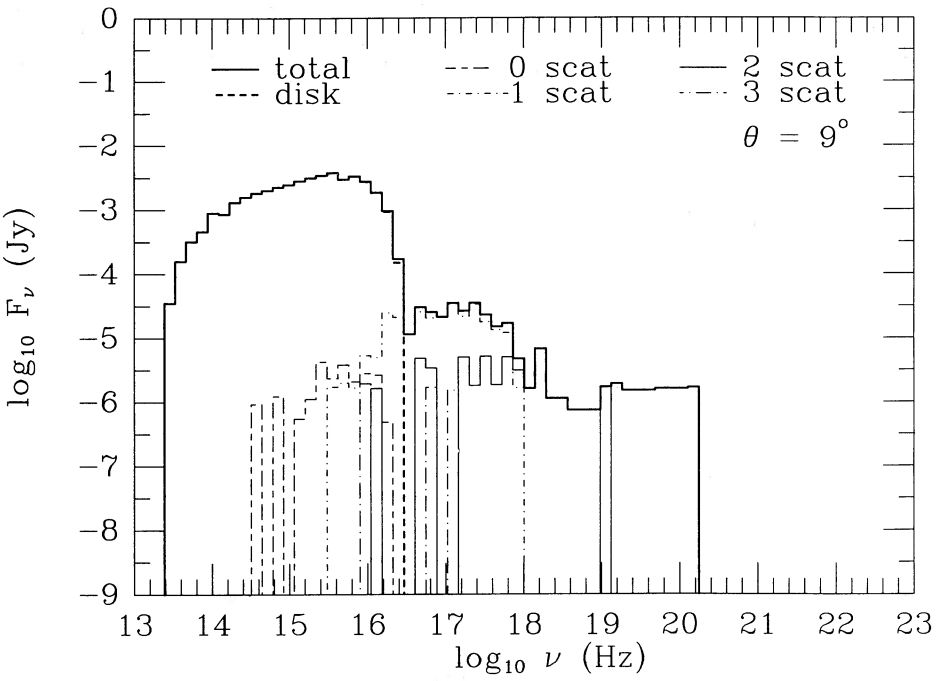


FIG. 6c

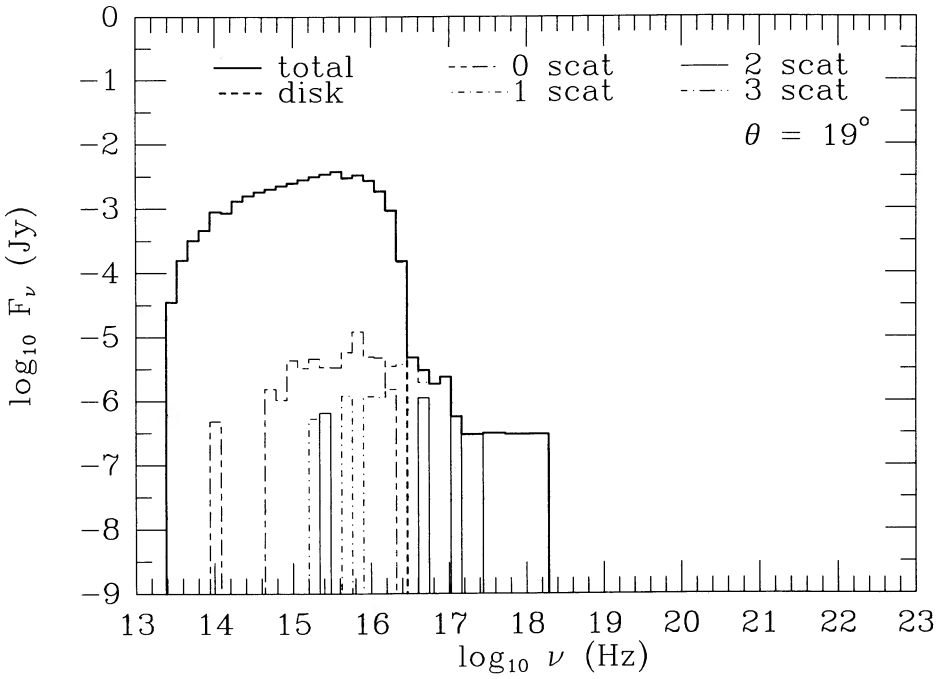


FIG. 6d

$\gamma_i m_e c^2$) ($\approx 3 \times 10^{22} h$ ergs in this example, where h is the Planck constant). The Monte Carlo simulation for the spectrum seen at $\theta = 0°$ (Fig. 6*a*) confirms this prediction. Figures 6*b*–6*d* also confirm the expectation that $\epsilon_{max}(\theta)$ should generally decrease as θ increases because the radiation beamed into the wider cones is upscattered in regions of lower γ. We note, however, that the detailed shape of the high-energy portion of the upscattered spectrum could be modified as a result of opacity effects, which tend to decrease the peak flux and increase the effective cutoff energy of the thermal emission from the disk (e.g., Czerny and Elvis 1987; Wandel and Petrosian 1988).

In addition to highlighting the dependence of ϵ_{max} on the viewing angle θ, Figures 6*a*–6*d* also demonstrate the variation of the spectral shape with θ. At small angles to the axis ($\theta \lesssim 1/\gamma_i$), only single scattering events contribute to the spectrum. In this case, the radiation is dominated by photons that are strongly beamed near the base of the jet, where $\gamma \approx \gamma_i$. A fraction of these photons

© American Astronomical Society • Provided by the NASA Astrophysics Data System

1989ApJ...340..162M

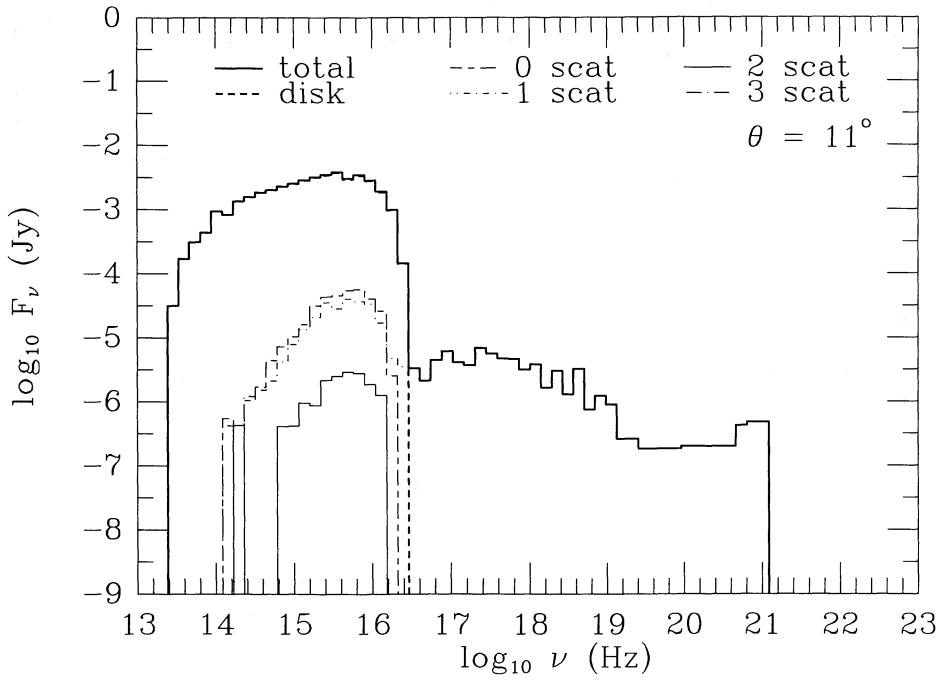


FIG. 7a

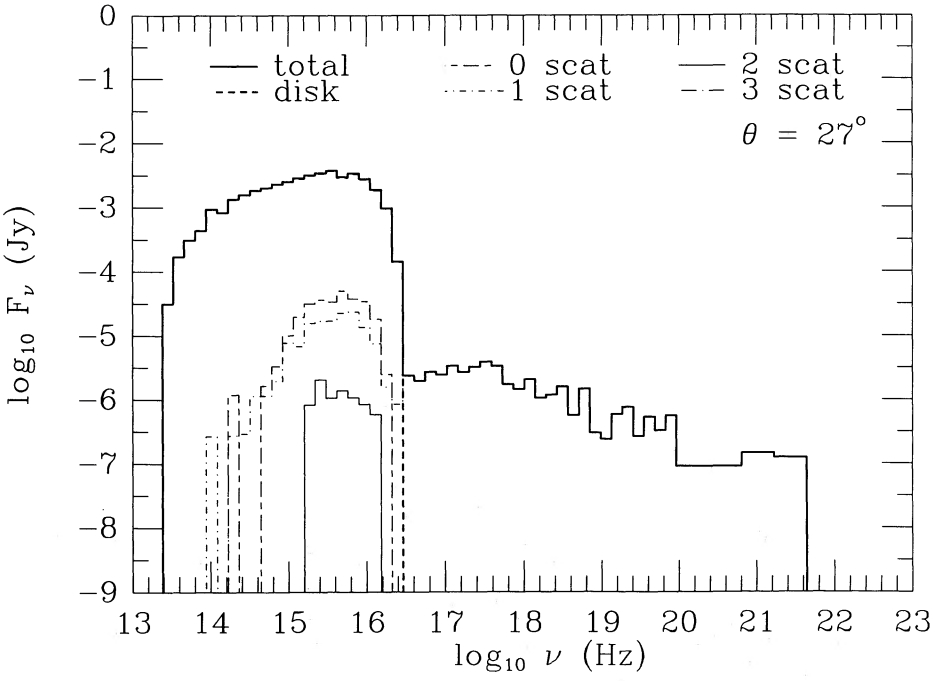


FIG. 7b

FIG. 7.—(*a*) Same as Fig. 6*a*, except that the jet has a fan geometry ($\delta = -2$) with a half-opening angle $\theta_j \approx 27°$, and is viewed at an angle $\theta = 11°$ to the axis. (*b*) Same as (*a*), except that the viewing angle is $\theta = 27°$. (*c*) Same as (*a*), except that the viewing angle is $\theta = 37°$. Note that $\theta > \theta_j$ in this case.

© American Astronomical Society • Provided by the NASA Astrophysics Data System

1989ApJ...340..162M

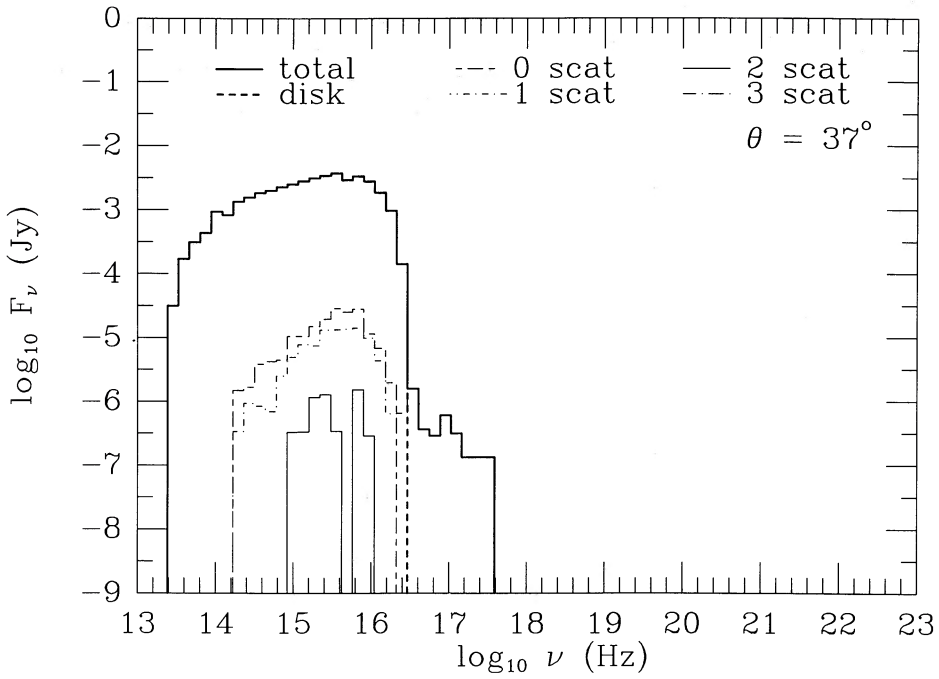


FIG. 7c

interact with the jet again, but these correspond to backward scattering events which both decrease the photons' energy and scatter them into a wider cone. It is evident from Figure 6*a* that the Comptonized spectrum observed along the axis is not simply a "boosted" thermal disk component (which would be the case if γ were uniform along the jet), but is rather flatter, and even slightly rising. The reason for this is that the γ distribution actually peaks at $z \approx z_b$ (see Fig. 3), which is also where the radiation from the disk is most intense. Hence, the $\theta \lesssim 1/\gamma_i$ spectrum, which is produced near the base of the jet, is dominated by the contribution of the most energetic particles and photons.

Away from the jet axis ($\theta \gtrsim 1/\gamma_i$), the upscattered radiation can be decomposed into two basic components: (1) a low-energy ($\epsilon \lesssim \gamma_\infty^2 \epsilon_{0,\,\max}$) component dominated by single scatterings and (2) a flatter component dominated by double (and sometimes triple)

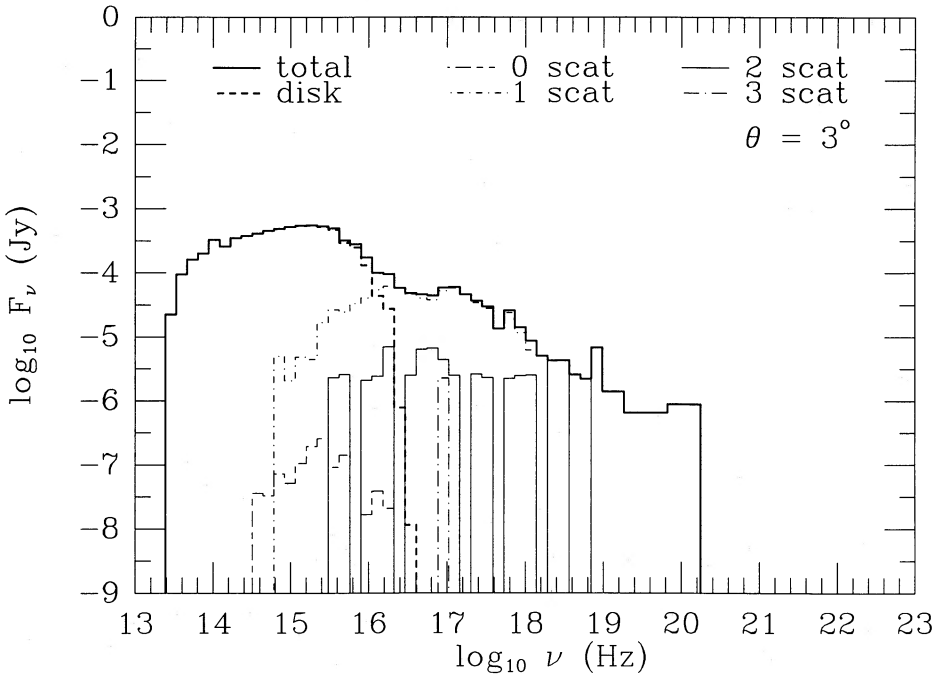


FIG. 8.—Comptonized spectrum arising from the upscattering of (thermal) disk radiation by the particles in a cylindrical ($\delta = 0$) e^-e^+ jet that is viewed at an angle $\theta = 3°$ to the axis, for a disk configuration specified by $R_{\rm in} = 5R_g$, $R_f = 50R_g$ (with $M = 10^8\ M_\odot$), $\theta_f = 90°$, and $T_{\max} = 10^5$ K. The jet is launched with an initial Lorentz factor $\gamma_i = 10^3$ at a height $z_b = 30R_g$, and has a radius $R_b = 5R_g$. The flux density is normalized as in Fig. 6.

© American Astronomical Society • Provided by the NASA Astrophysics Data System

1989ApJ...340..162M

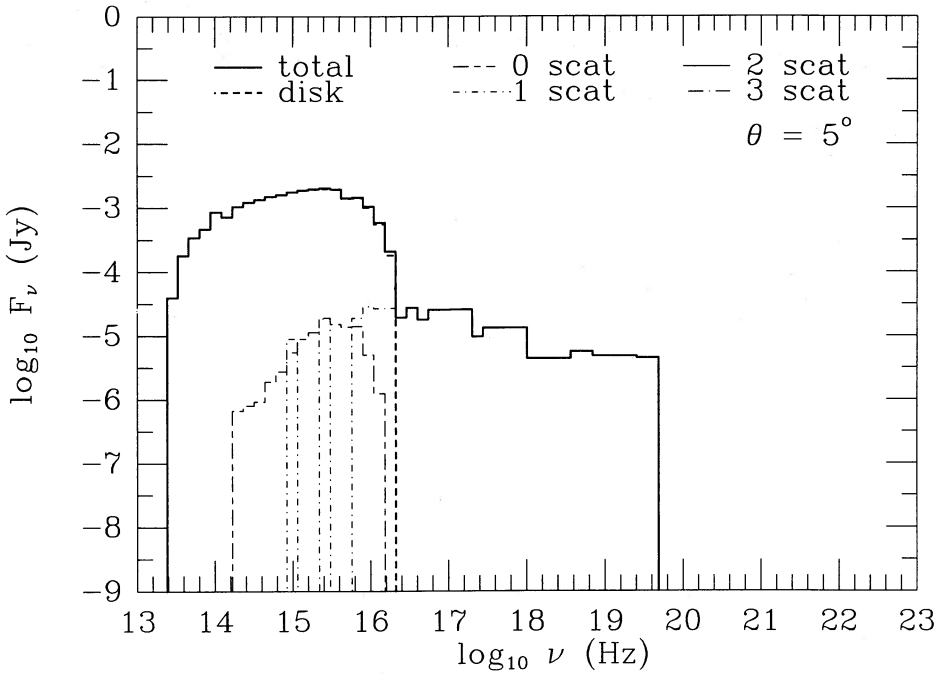


FIG. 9.—Comptonized spectrum arising from the upscattering of (thermal) disk radiation by the particles in a fan ($\delta = -2$) e^-e^+ jet of half-opening angle $\theta_j \approx 27°$ that is viewed at an angle $\theta = 5°$ to the axis. The disk configuration is specified by $R_{in} = 5R_g$, $R_f = 50R_g$ (with $M = 10^8 M_\odot$), $\theta_f = 90°$, and $T_{max} = 1.5 \times 10^5$ K. The jet is launched at a height $z_b = 75R_g$ with an initial Lorentz factor $\gamma_i = 10^3$ and base radius $R_b = z_b/2$. The flux density is normalized as in Fig. 6.

scatterings extending to higher energies. In this case, the spectral shape of component 1 does mimic that of the thermal radiation from the disk because these scattering events take place beyond the strong deceleration zone at the base of the jet. Thus, component 1 is not only scattered into a wider cone (because of the lower γ), but also exhibits fewer modifications to the boosted thermal spectrum because the variations in γ are less extreme (see Fig. 3). Component 2, on the other hand, constitutes the multiply scattered radiation that was first intercepted at the base of the jet. The initial scattering by particles with $\gamma \approx \gamma_i$ is responsible for the relatively high photon energies and induces strong beaming along the jet axis. This initial beaming, in turn, increases the probability for higher order scatterings that eventually deflect the photons in the observer's direction.

We can summarize the qualitative features of the spectra shown in Figures 6*a* and 6*b* as follows: At very small viewing angles ($\theta \lesssim 1/\gamma_i$), the upscattered spectrum is dominated by photons that are singly scattered at $z \approx z_b$, and is relatively flat all the way out to the cutoff frequency $\epsilon_{max}/h \approx 3 \times 10^{22}$ Hz because the scattering probability distribution is biased in favor of the most energetic particles and thermal photons. At viewing angles larger than $\sim 1/\gamma_i$, the multiple scattering component is dominant beyond the frequency $\gamma_\infty^2 \epsilon_{0,max}/h \approx 2 \times 10^{18}$ Hz, where the single scattering component (produced by $\gamma \approx \gamma_\infty$ particles) steepens. Thus, away from the jet axis, the spectrum consists of a shifted thermal hump and a flat high-energy tail. In addition, both the flux level and the cutoff energy decrease as θ increases because of the weaker Doppler boosting at larger angles.

Many of the characteristics described above are also evident in the spectra produced by a fan jet ($\delta = -2$), though there exist several important differences. Figures 7*a*–7*c* show representative spectra arising from the Compton-drag interaction in fan e^-p jets. Other than δ, the model parameters are the same as those in Figure 6. In this case, very few multiple scattering events contribute to the spectrum because of the smaller optical depth along the jet. Also, because we assumed a radial outflow, the spectrum is essentially independent of viewing angle as long as $\theta \lesssim \theta_j$, where θ_j ($\approx 27°$ in this example) is the jet half-opening angle. Outside the jet cone, the dependence of the spectral features on the angle $(\theta - \theta_j)$ is similar to the dependence on θ in the case of a parallel jet (Fig. 6). In particular, both the flux and the cutoff energy decrease rapidly when $(\theta - \theta_j)$ increases beyond $\gtrsim 1/\gamma_i$.

For comparison, Figures 8 and 9 show representative spectra from parallel and fan electron-positron jets, respectively. These jets decelerate much faster than electron-proton jets because of their smaller mean mass per particle. In order for γ_∞ to remain high, the intensity along the jet axis must, therefore, be lower. Such a reduction could be brought about by a lower disk temperature, a flatter geometry (i.e., $\theta_f \to 90°$), or a larger z_b. Our calculations indicate that a combination of all three effects is required to produce an e^-e^+ jet with a terminal Lorentz factor $\gamma_\infty \approx 10$. For example, in Figure 8 we assume $T_{max} = 1 \times 10^5$ K, $\theta_f = 90°$, and $z_b = 30R_g$. The other parameters are the same as those of Figure 6 with one crucial difference: when we attempt to model the Comptonized spectrum for a source like PKS 2155−304 by using the synchrotron luminosity to constrain the jet power, we find

$$\tau_\perp \approx 0.5\left(\frac{R_b}{15R_g}\right)^{-1}\left(\frac{M}{10^8\ M_\odot}\right)^{-1}\left(\frac{F_s}{2 \times 10^{-9}\ \text{ergs cm}^{-2}\ \text{s}^{-1}}\right)\left(\frac{D}{1\ \text{Gpc}}\right)^2\left(\frac{\gamma_\infty}{10}\right)^{-5}\left(\frac{\varepsilon}{0.5}\right)^{-1}\left(\frac{m}{m_e}\right)^{-1}$$

(see eq. [30]). In other words, an e^-e^+ jet starting below $z_b \approx 30R_g$ must be optically thick unless the efficiency ε is unreasonably large. However, if the jet is indeed optically thick, the Compton-drag mechanism will not be able to decelerate it. The calculation of

© American Astronomical Society • Provided by the NASA Astrophysics Data System

1989ApJ...340..162M

the spectrum in Figure 8 assumes an efficiency $\varepsilon = 0.5$, corresponding to a transverse optical depth $\tau_\perp \approx 0.5$. This difficulty aside, we see from this figure that the qualitative features of the spectrum are similar to those of a parallel e^-p jet. In particular, the "boosted" thermal hump is evident, as is the flattening toward the cutoff frequency. Again, the high-energy tail is primarily due to multiply scattered photons.

The apparent difficulty with $\tau_\perp$ (or ε) can be alleviated by starting the e^-e^+ jet farther from the black hole. In fact, it could be that the effective value of z_b in such jets is determined by the condition $\tau_\perp \approx 1$. However, for any given value of γ_i, there is an upper limit on z_b beyond which an e^-e^+ jet cannot be decelerated to a terminal Lorentz factor $\gamma_\infty \approx 10$ (see Fig. 4*b*). Figure 9 shows an illustrative spectrum arising from inverse Compton scattering in a fan e^-e^+ jet starting at $z_b = 75R_g$. In this case, $T_{\max} = 1.5 \times 10^5$ K and $\theta_f = 90°$. The other parameters are the same as in Figure 7. Even at this base height, ε must be $\gtrsim 0.1$ in order for $\tau_\perp$ to remain $\lesssim 1$. The qualitative features of this spectrum are similar to those of Figure 7, except that at any given angle the cutoff energy is lower. This is because both z_b and θ_f are larger in this case, so the scattering between the thermal photons and the particles in the jet takes place at larger incidence angles.

IV. APPLICATIONS

a) Kinematic Properties of Relativistic Jets

The detailed calculations described in § III*a* have confirmed the suggestion (Phinney 1987) that the thermal radiation field associated with nuclear AGN disks should be very effective in decelerating ultrarelativistic jets. In fact, using the particle equation of motion (eq. [10]), the criterion for the deceleration of an optically thin jet that is injected near the inner edge of a flat disk can be expressed as

$$\gamma_i \left(\frac{\sigma}{\sigma_T}\right)\left(\frac{m_e}{m}\right) l_{\rm disk} \gtrsim 1$$

(where $l_{\rm disk} \equiv L_{\rm disk}\sigma_T/4\pi m_e c^3 R_{\rm in}$ is the nominal *compactness parameter* of the disk and $L_{\rm disk}$ is the total escaping luminosity), which demonstrates explicitly that the deceleration efficiency *increases* with the initial Lorentz factor γ_i in the Thomson scattering regime (see Fig. 4). Since $l_{\rm disk} = 67\,(L_{\rm disk}/2 \times 10^{45}\ {\rm ergs\ s^{-1}})(R_{\rm in}/7 \times 10^{13}\ {\rm cm})^{-1}$ (evaluated for a disk with $M = 10^8\ M_\odot$, $R_{\rm in} = 5R_g$, and $T_{\max} = 10^5$ K) is typically much greater than unity, this criterion would be satisfied for all e^-e^+ jets as well as for e^-p jets with moderately high initial Lorentz factors. As is evident from Figure 3, the deceleration is even stronger in the case of thick disks that possess a central funnel. When γ_i is much larger than $\gamma_{\rm KN} \equiv m_e c^2/k_B T_{\max} \approx 6 \times 10^4 (T_{\max}/10^5\ {\rm K})^{-1}$, σ/σ_T decreases to the Klein-Nishina value $\sim \gamma_{\rm KN}/\gamma_i$ and the deceleration efficiency no longer increases with γ_i. However, even in this limit the Compton-drag mechanism can decelerate outflows with arbitrarily large values of γ_i, provided only that the optical depth across the jet satisfies $\tau_\perp \lesssim 1$.

The mean value of the apparent expansion speed (in units of c) in the currently cataloged superluminal radio sources is $\sim(6 \pm 5)h_0^{-1}$, with no reported measurement exceeding $20h_0^{-1}$ (Porcas 1987). On the assumption that these sources are observed at a Doppler-favored angle (e.g., Blandford and Königl 1979), the inferred expansion speed can be identified with the terminal Lorentz factor γ_∞ of the associated relativistic jet. As we have found from our model calculations (see Figs. 4*a* and 4*b*), the value of γ_∞ depends on the maximum disk temperature $T_{\max}$, the height z_b of the base of the jet, and the black hole mass M, although it is rather insensitive to the value of γ_i. Is it then possible to account with this model for the relatively narrow range inferred for γ_∞? To provide an illustrative answer to this question, we assume, for simplicity, that the black holes associated with the observed relativistic jets have been assembled by disk accretion over a constant period of time $t_a \equiv M/\dot{M}$ ($\approx 2.5 \times 10^8$ yr for the fiducial disk parameters adopted above). Now, the deceleration equation for a jet with $\gamma_i \gg 1$ and $z_b/R_{\rm in} \gg 1$ in the radiation field of a flat disk can be approximated by

$$mc^3 \frac{d\gamma}{dz} = -\frac{\kappa\sigma L_{\rm disk} R_{\rm in}}{2\pi z^3}\gamma^2 ,$$

where $\kappa \approx 0.08$ is a structural constant (see Phinney 1987 as well as eqs. [1] and [10]). This equation indicates that, as long as the deceleration distance is $\gtrsim z_b$, the terminal Lorentz factor is given approximately by

$$\gamma_\infty \approx \frac{1}{\kappa l_{\rm disk}}\left(\frac{m}{m_e}\right)\left(\frac{z_b}{R_{\rm in}}\right)^2 ,$$

where we set $\sigma = \sigma_T$. Using equation (22) for $L_{\rm disk}$ and substituting $\dot{M} = M/t_a$, we obtain $\gamma_\infty \approx 6(\kappa/0.08)^{-1}(m/m_e)(t_a/2.5 \times 10^8\ {\rm yr})(z_b/30R_g)^2$, in good agreement with the exact result for these parameter values. It follows that, to the extent that t_a and (z_b/R_g) remain constant, the asymptotic Lorentz factor should be uniform from source to source even though the values of M, $R_{\rm in}$, z_b, and $T_{\max}$ could separately vary. [With the above scaling, the variation of $T_{\max} = 10^5\,(M/10^8\ M_\odot)^{-1/4}(t_a/2.5 \times 10^8\ {\rm yr})^{-1/4}(R_{\rm in}/5R_g)^{-3/4}$ K would, however, be relatively weak.] The above expression for γ_∞ also suggests that the observed superluminal sources are likely to be associated with e^-e^+ rather than with e^-p jets, although this conclusion will be mitigated if the disks are thick (see Fig. 3). In addition, the approximate solution to the equation of motion confirms the result of the numerical calculation that γ_∞ is largely independent of γ_i (see Fig. 4).

On the basis of our detailed calculations in §§ II and III and the simple $t_a = $ const. scenario outlined in the preceding paragraph, we conclude that a narrow distribution of terminal Lorentz factors which is consistent with the observations of superluminal radio sources can arise quite naturally in the context of the proposed interaction between an initially hyperrelativistic jet and the thermal

© American Astronomical Society • Provided by the NASA Astrophysics Data System

1989ApJ...340..162M

radiation field from an AGN accretion disk. In particular, we have found that the jet can emerge from the deceleration region with a finite Lorentz factor that lies in the inferred range even if no additional acceleration by some external agent is applied in that zone (which contrasts with a statement to this effect in Begelman and Sikora 1987). However, the observed range of γ_∞ could also be associated, at least in part, with a selection effect. Sources with comparatively luminous disks (corresponding to small values of t_a) would have weakly beamed jets ($\gamma_\infty \approx 1$) that may remain undetected. Conversely, jets in faint disk sources (large t_a) or with large mass discharges (corresponding to $\tau_\perp \gg 1$ near the base of the flow) would have $\gamma_\infty \gg 1$ and could go unobserved simply because their emission would be Doppler-focused into a very narrow beam (see Phinney 1987 for further discussion of this point). Clearly, such a selection effect would complicate any conclusions that might be drawn from the statistics of these sources. For example, blazar sources have commonly been interpreted as the beamed "tail" of a much larger, intrinsically faint parent population (e.g., Angel and Stockman 1980). If the radiative deceleration scenario is applicable to most of these objects, then it is possible that blazars are observed *because* they are associated with faint sources that have relatively weak disk emission, and that even fainter sources are not observed because their associated jets remain too strongly beamed.

Another aspect of the proposed deceleration scenario that may have interesting astrophysical implications is the expected transverse gradient in the asymptotic velocity distribution of the particles in the jet (see Fig. 5). This effect is most pronounced in the case of a fan jet or in a disk with a central accretion funnel, although a similar transverse gradient will also form in a parallel jet if $\tau_\perp$ is nonnegligible. A systematic decrease in γ_∞ with distance from the axis of the jet could help alleviate some of the difficulties that are encountered when one attempts to unify various properties of radio sources and quasars using a single-velocity, unidirectional, relativistic beam model. In particular, there is mounting observational evidence (e.g., Barthel *et al.* 1988) for the absence of a direct correspondence between the overall orientation of extended radio quasars and either the occurrence of superluminal motions in their cores or the relative core brightness, contrary to the predictions of the simple model. These difficulties, as well as the related problem of a significant apparent misalignment between the small-scale and the large-scale structure in several strong radio sources, could be relieved if AGN jets have broad ejection cones and a radially decreasing distribution of Lorentz factors, as originally proposed by Rees (1981). Although this suggestion has been subject to certain criticisms (e.g., Readhead, Pearson, and Barthel 1988), it nevertheless remains an attractive way for resolving at least some of the difficulties with the basic beaming hypothesis. As our calculations have demonstrated, a wide-cone jet that interacts with the radiation field of a surrounding disk will naturally develop a monotonic velocity gradient in the desired sense even if the initial distribution of γ_i were uniform across the beam. The predicted velocity distribution might also be relevant to the interpretation of superluminal radio sources such as 3C 345 (Biretta, Moore, and Cohen 1986) and 3C 273 (Cohen *et al.* 1987) in which different components appear to move with different velocities as well as in different projected directions. In light of the fact that the apparent velocity depends sensitively on the viewing angle (see Fig. 1 in Cohen and Unwin 1984), the observed velocity dispersion may simply correspond to the different emission components moving along different directions in the jet and does not require that their actual speeds also vary. However, for a constant Lorentz factor $\gamma_\infty \lesssim 10$, the observed variations in the apparent speed would imply significant differences in the corresponding Doppler factors and hence in the flux densities of the moving components, whereas the measured flux differences are relatively small. This discrepancy could be alleviated if the measured components move in a fan jet with a nonuniform γ_∞ distribution as predicted in our model. In that case, the increase in the viewing angle (for an observer located outside the ejection cone of the jet) would be compensated for by an increase in the Lorentz factor, so the apparent velocity could change while the Doppler factor would remain nearly constant (see Fig. 1 in Blandford and Königl 1979). According to this interpretation, the apparent velocity should *increase* with the viewing angle, so the faster components would be predicted to move closer to the axis of the jet.

b) The Hard X-Ray Component in BL Lac Objects

There now exists substantial observational evidence that the X-ray emission in BL Lac objects can often be decomposed into two components: a steep spectrum with energy spectral index $\alpha \gtrsim 1$ at low energies, and a hard ($0 < \alpha < 1$) component above a few keV (e.g., Urry, Mushotzky, and Holt 1986). Some reported measurements are even consistent with a negative spectral index for the higher energy component (e.g., Mushotzky *et al.* 1978; Hall *et al.* 1981; Urry and Mushotzky 1982), but, in any case, the absence of detectable high-energy γ-rays in these sources (e.g., Bignami *et al.* 1979) indicates that the spectrum must steepen again somewhere between ~ 10 keV and ~ 100 MeV. The hard X-ray component appears to be the more highly variable of the two, frequently exhibiting large intensity changes between successive observations that are separated by several weeks or months (e.g., Mushotzky *et al.* 1979; Makino *et al.* 1987). Direct measurements have shown, however, that flux changes on time scales as short as 30 s can occur in these objects in both the infrared (Wolstencroft, Gilmore, and Williams 1982) and X-ray (Feigelson *et al.* 1986) regimes. Although the presence of a hard X-ray component has not been confirmed by either the *EXOSAT* satellite (Barr *et al.* 1989) or, to this date, the *Ginga* experiment (Ohashi 1989), this is not necessarily in conflict with the reported *HEAO* 1, *HEAO* 2, and *Tenma* detections in view of the limited spectral sensitivity of *EXOSAT* and the relatively short measurements conducted so far with *Ginga*. Sustained observations with the latter satellite will be of great importance for resolving this issue.

The soft, generally less variable, X-ray component appears to be a smooth continuation of the ultraviolet spectrum of BL Lac objects. This component has been interpreted as part of the beamed synchrotron emission from the associated relativistic jet. In fact, the entire "generic" spectrum from the radio to soft X-rays can be modeled in terms of synchrotron radiation from an inhomogeneous, conical jet that is observed at a small angle to the axis (e.g., Königl 1981). The hard X-ray component, in turn, has been explained as the self-Compton emission from the jet. In the context of the inhomogeneous jet model, it is possible to account for the apparently rising hard X-ray spectrum in a source like PKS 2155−304 in terms of once-scattered inverse Compton radiation from the innermost (and presumably more highly variable) optically thin region in the jet (e.g., Urry and Mushotzky 1982). However, this spectral fit depends on identifying the break frequency of the synchrotron emission spectrum in that region with the apparent bend in the optical spectrum of this source (see Fig. 10), which has the consequence that the model then cannot adequately account for the bulk of the measured radio spectrum (cf. Worrall *et al.* 1984). If the break frequency is associated instead with the apparent bend in

© American Astronomical Society • Provided by the NASA Astrophysics Data System

1989ApJ...340..162M

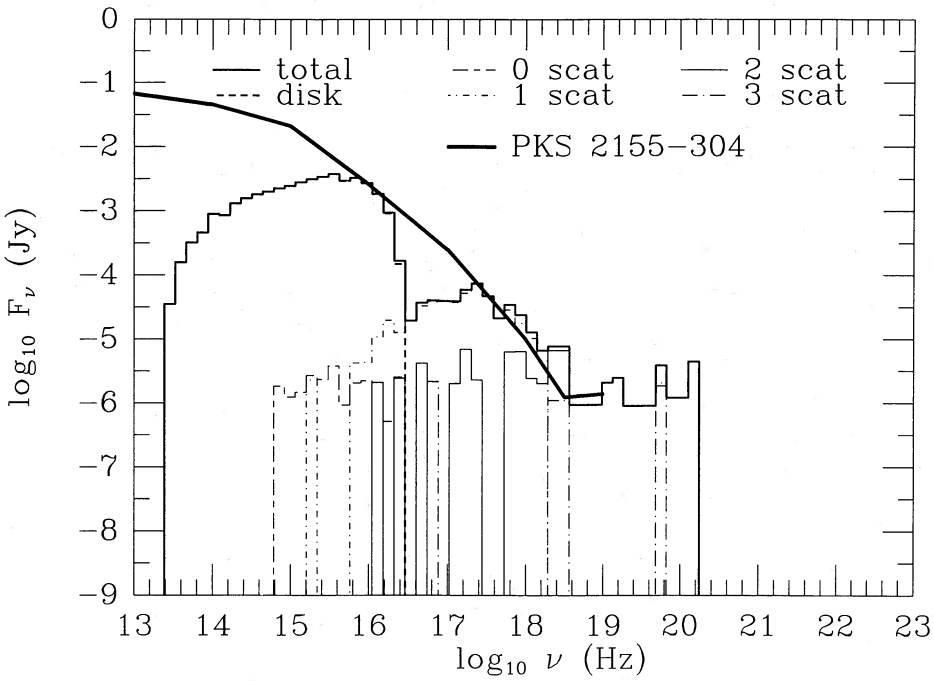


FIG. 10.—Comptonized spectrum calculated with the parameters of Fig. 6*a* (but for a viewing angle $\theta = 7°$ with respect to the jet axis) superposed on a fit (*heavy line*) to the spectrum of the BL Lac object PKS 2155−304 (using data from Urry and Mushotzky 1982).

the radio spectrum of PKS 2155−304, then it is possible to incorporate the entire radio spectrum into the model fit, but the predicted inverse Compton emission becomes too weak (and its spectral index too large) to match the observed hard X-ray component (see Fig. 2 in Königl 1981). A similar difficulty in accounting for the entire observed spectrum in terms of synchrotron self-Compton emission from a geometrically simple outflow is encountered also in other versions of the inhomogeneous jet model (e.g., Ghisellini, Maraschi, and Treves 1985).

The aforementioned difficulty with the self-Compton interpretation leads us to suggest an alternative explanation of the hard X-ray component in BL Lac sources, namely, that it represents the inverse Compton emission produced in the course of the interaction between the associated relativistic jet and the thermal radiation field of the nuclear accretion disk. In Figure 10 we show an illustrative fit to the high-energy X-ray spectrum of PKS 2155−304 using representative disk and jet parameters. It is seen that the predicted optical through soft X-ray flux from the disk does not exceed the measured flux (attributed to the beamed synchrotron emission from the jet). On the assumption that $R_{\rm in}/R_g$ and t_a are approximately constant (see § IV*a*), the flux from the disk should scale as M and could, in principle, contribute to the measured emission from a source with a large central mass. In fact, a direct detection of a UV "bump" has already been reported in the "superluminal" quasar 3C 345 (Bregman *et al.* 1986) as well as in several other highly polarized quasars (e.g., Malkan and Moore 1986), and the presence of a thermal emission component in this class of blazars has also been inferred from the apparent wavelength dependence of the degree of polarization in these sources (Smith *et al.* 1986, 1988; Wills 1989). However, there is no conclusive evidence yet for a "big bump" component in BL Lac objects. For example, the apparent absence of this component in a source like PKS 0548−322 (Urry *et al.* 1982), where the flux density at $\sim 10^{15}$ Hz is over an order of magnitude lower than in PKS 2155−304 and the inferred distance is a factor ~ 7 smaller, can be used to argue that the mass accretion rate $\dot{M}$ in this object is significantly lower than in PKS 2155−304. In our model fit to PKS 2155−304, the disk emission can marginally account for the measured UV flux density, and in the analogous disk model of Wandel and Urry (1989), the entire UV through soft X-ray spectrum of this source is attributed to thermal radiation. (The latter interpretation could in principle be tested by future X-ray polarization measurements.) On the basis of our dynamical calculations, we expect that luminous disks would be relatively more efficient in decelerating ultrarelativistic jets (see § IV*a*). Thus we predict that, if the presence of a "big bump" component in BL Lac objects is eventually confirmed, then the strength of this emission should be directly correlated with that of the hard X-ray component produced in the course of the jet deceleration. In sources where the deceleration process takes place, the upscattered X-ray flux scales as $L_{\rm jet}/\max(\theta_j^2, \gamma_\infty^{-2})$. The fact that the measured flux density of the hard X-ray component in BL Lac objects is typically $\gtrsim 10^{-6}$ Jy at frequencies $\gtrsim 10^{18}$ Hz is then consistent with the jet parameters being approximately the same in these sources.

The flat high-energy spectra predicted by our model (see § III*b*) provide a natural explanation for the shape of the hard X-ray component measured in the most X-ray–bright BL Lac objects (Urry, Mushotzky, and Holt 1986). This emission can be interpreted in either of two ways: (1) In a parallel jet, it most likely represents the multiply scattered photons that are observed away from the jet axis ($\theta > 1/\gamma_i$) but still within the emission cone of the decelerated jet ($\theta \lesssim 1/\gamma_\infty$). (2) In a fan jet observed at an angle $\theta \lesssim \theta_j$, this component corresponds to singly scattered photons originating relatively close to the base of the jet. [For a fan jet observed at an angle $\theta > (\theta_j + 1/\gamma_i)$, the interpretation is similar to that for a parallel flow.] These two alternatives lead to different predictions for the high-energy cutoff of the spectrum. In the case of a fan jet with $\theta \lesssim \theta_j$, the cutoff energy extends to $\min(\gamma_i^2 \epsilon_{0,\max}, \gamma_i m_e c^2)$ and is

© American Astronomical Society • Provided by the NASA Astrophysics Data System

1989ApJ...340..162M

independent of θ (see Fig. 7). For a parallel jet [or a fan jet with $(\theta - \theta_j) > 1/\gamma_i$], the cutoff occurs at lower energy and decreases with increasing θ (see Fig. 6). As we noted at the beginning of this subsection, a steepening of the hard X-ray component is required for consistency with the high-energy γ-ray measurements. However, the observations carried out so far do not constrain the detailed shape of the spectrum in the range ~ 10 keV–100 MeV.

The proposed model also accounts naturally for the strong variability of the high-energy X-ray component, which can be associated with the expected "jitter" in the jet deceleration zone. Because of the large gradients in the particle Lorentz factors in that region, any small changes in the ejection angle could lead to strong variations in the measured flux that originates from there. Similar variability could result from a nonsteady ejection of discrete emission components, for which there is, in fact, evidence from optical polarimetric studies of BL Lac (Moore, Schmidt, and West 1987). If we identify the measured variability time scale $t_{\rm var}$ with the deceleration time measured by an observer located within the beaming cone of a parallel jet ($\gamma_\infty^2\,\theta^2 < 1$), we obtain the estimate

$$t_{\rm var} \approx (1/4\kappa l_{\rm disk})(z_b/\gamma_\infty R_{\rm in})^3(R_{\rm in}/c) \approx 24(\kappa/0.08)^{-1}(L_{\rm disk}/2\times 10^{45}\ {\rm ergs\ s^{-1}})^{-1}(z_b/6R_{\rm in})^3(\gamma_\infty/10)^{-3}(R_{\rm in}/7\times 10^{13}\ {\rm cm})^2\ {\rm s}$$

(see § IV*a*), where we assumed $m = m_e$ and $\sigma = \sigma_{\rm T}$. This estimate is consistent with the shortest reported X-ray variability time scale (Feigelson *et al.* 1986). We note, however, that our model does not predict comparably low values of $t_{\rm var}$ at low frequencies, so the 30 s infrared variations reported in OJ 287 (Wolstencroft, Gilmore, and Williams 1982) must be interpreted in another way. (An explanation in terms of relativistic shocks propagating in the jet would also fail in that respect because of Compton-loss constraints; see Marscher and Gear 1985.) We also observe that the expected time variability of the upscattered disk emission is consistent with the behavior of the X-ray spectra measured by *EXOSAT*, which exhibit a larger variability amplitude at higher frequencies and a smaller spectral index at higher intensities (e.g., Maraschi and Maccagni 1988). In this picture, the convex shape of the *EXOSAT* spectra (Barr *et al.* 1989) may be associated with the tail of the shifted thermal hump predicted in our model for viewing angles $\theta \gtrsim 1/\gamma_i$ (see § III*b* and Fig. 10). The *EXOSAT* data may thus provide indirect support for this model even though the observed energy range is apparently too narrow to test the two-component nature of the predicted spectrum.

The total inverse Compton luminosity emitted by the decelerated jet is of the order of the initial kinetic power of the outflow and is typically much larger than the synchrotron luminosity from the jet (see eq. [27]). The fact that the measured values of $(\nu F_\nu)_{\rm synchrotron}$ and $(\nu F_\nu)_{\rm hard\ X\text{-}rays}$ in the most X-ray–bright BL Lac objects are typically comparable (see Fig. 10) is, of course, perfectly understandable in our model, which predicts that most of the power given up by the jet appears at substantially higher energies. Specifically, in the case of a parallel jet, most of the power is emitted within an angle $1/\gamma_i$ from the axis and is concentrated near the upper cutoff in the spectrum (see Fig. 6*a*), and even at larger observation angles the value of (νF_ν) often peaks well beyond the hard X-ray regime (Figs. 6*b* and 6*c*). In the case of a uniform fan jet observed at an angle $\theta \lesssim \theta_j$, the power per unit solid angle does not vary strongly with θ (except at large angles where the deceleration is more efficient), but the specific luminosity is still maximized near $\epsilon_{\rm max}$ (see Figs. 7*a* and 7*b*).

The preceding considerations imply that, if most relativistic jet sources are of the "parallel" variety, then it is possible that a sufficiently faint survey would uncover an object that is seen at an angle $\lesssim 1/\gamma_i$ to the axis and whose high-energy spectrum therefore corresponds to Figure 6*a*. [On the assumption that the jet axes are randomly oriented, such an object would be a factor $\sim(\gamma_\infty/\gamma_i)^2$ less likely to be found than a source like PKS 2155−304, although this would be partially compensated by its relative brightness; cf. Figs 6*a* and 10.] Although no BL Lac object has yet been identified as a γ-ray source, the high-energy emission from this class of sources is, nevertheless, constrained by the measured diffuse γ-ray background (e.g., Bignami *et al.* 1979). In particular, the relatively steep spectrum ($\alpha \approx 1.7$) of the background radiation above a few MeV implies that it cannot be attributed to the flat-spectrum inverse Compton emission predicted by our model. Simple estimates based on our fit to PKS 2155−304 and the inferred contribution of BL Lac objects to the diffuse X-ray background indicate that our model spectra are consistent with this constraint, provided that the values of $L_{\rm jet}$ and γ_i are not much larger than those that we have adopted.

In describing the radiative deceleration of ultrarelativistic jets, we have presented results for both parallel and fan jets. Possible support for the relevance of the fan geometry is provided by the observation that X-ray–selected BL Lac objects have comparable X-ray luminosities but lower radio and UV luminosities than radio-selected BL Lac objects, which has been interpreted to imply that the X-ray emission in these sources is more isotropic than the radiation at lower frequencies (Stocke *et al.* 1985; Maraschi *et al.* 1986; Worrall 1987). In the context of our model, this situation could arise if the jets were initially ejected in a wide cone and were subsequently collimated, or if only the material near the axis of the cone could overcome the gravitational pull of the central mass (on account of its higher value of γ_∞) and avoid impacting on the accretion funnel's wall. Under these circumstances, the hard X-ray component arising from the radiative deceleration of the initial outflow would be emitted into a wider solid angle than the synchrotron radiation produced farther out in the collimated jet. However, despite their greater isotropy, these high-energy X-rays would still be strongly beamed.

Finally, we comment on the implications of our model for nonblazar AGNs. In the application of the beaming hypothesis to QSOs (e.g., Blandford and Königl 1979), core-dominated radio-loud quasars are interpreted as relativistic jet sources that are observed with $\theta\gamma_\infty \lesssim 1$, so that the observer is located within the emission cone of the beamed synchrotron radiation from the jet. There is now growing evidence that the distinction between radio-quiet and radio-loud QSOs extends also to the low-energy X-ray regime, with the former characterized by a steep ($\alpha \approx 1$) X-ray spectrum and the latter having a flatter ($\alpha \approx 0.5$) X-ray emission component (e.g., Wilkes and Elvis 1987). A possible interpretation of the $\alpha \approx 0.5$ component in the context of the radiative deceleration model is that it represents the Compton-upscattered thermal emission from the associated accretion disk. In particular, the measured spectral index could correspond to the singly scattered photons in a parallel jet that is observed at an angle $> 1/\gamma_i$ to the axis (see Fig. 6*b*, 6*c*, and 8). We emphasize, however, that inasmuch as BL Lac objects represent the most strongly beamed relativistic jet sources, they are expected to show the strongest evidence for the upscattered thermal radiation predicted by this model.

© American Astronomical Society • Provided by the NASA Astrophysics Data System

1989ApJ...340..162M

V. CONCLUSIONS

In this paper we have carried out detailed calculations of the expected interaction between an ultrarelativistic jet and the thermal radiation field produced by accretion onto a massive black hole. Extremely relativistic jets might be formed in the immediate vicinity of the hole by electromagnetic or hydromagnetic means, and the subsequent Compton-drag deceleration by the ambient radiation field could be the main reason why the apparent speeds measured in superluminal radio sources generally do not exceed $\sim 10h_0^{-1}c$ (Phinney 1987). In order to study this interaction, we adopted the basic disk model that has been invoked to account for the optical through soft X-ray emission in "unbeamed" quasars. Our simple representation of the geometry (flat surface plus conical funnel) and spectrum (sum of blackbodies) of the disk was motivated by a desire to make the calculation as transparent as possible, but we have tried to include most of the relevant effects (including the intensity enhancement due to internal reflections in the central funnel). Our representation of the jet geometry (straight cylinder or truncated fan) and the neglect of finite-$\tau_\perp$ effects were again intended for simplification. However, within the framework of this model, our calculation of the jet deceleration and of the spectrum produced by the Compton interaction is exact. In fact, the computational tools that we have developed can be readily applied also to other astrophysical problems of a similar nature.

Our results have allowed us to construct a self-consistent picture of the kinematic and spectral properties of radiatively decelerated e^-p and e^-e^+ relativistic jets. We have found that terminal Lorentz factors $\gamma_\infty \lesssim 10$ arise quite naturally in this picture for a variety of plausible disk and jet parameters, with no additional forces having to be invoked after the jet starts to decelerate. We noted that it is possible to account for the inferred uniformity of γ_∞ in the superluminal radio sources if the central masses in these objects were assembled by accretion over comparable time scales, but that the measured range of γ_∞ might be influenced by an observational selection effect. We also discovered that the proposed deceleration mechanism leads to a nonuniform distribution of γ_∞ across the jet, particularly in the case of disks with narrow funnels and fan-shaped outflows. The predicted radial decline of γ_∞ could facilitate the formulation of a unifying classification scheme for radio sources and quasars, and it could also be relevant to the interpretation of superluminal radio sources such as 3C 345 and 3C 273 in which different components move with different apparent velocities.

We suggested that the beamed inverse Compton emission that is produced in the course of the jet deceleration process could be detected in sources where the jet is observed at a small angle to the axis, and we proposed that this could be the origin of the hard X-ray component that has been measured in several BL Lac objects. We argued that this mechanism could account for the occurrence of flat or rising X-ray spectra in several of the most X-ray–bright BL Lac objects and for the rapid variability of the X-ray fluxes from these sources. We demonstrated that it is possible to model the X-ray spectrum of a source like PKS 2155−304 in this fashion without violating the constraint that the measured thermal radiation from the disk should not exceed the beamed synchrotron emission from the jet. We noted, however, that if the hypothesized thermal emission component is eventually measured in these sources, then its strength may be expected to correlate with that of the hard X-rays. According to this model, the hard X-ray component should terminate in a sharp cutoff, with the precise value of the cutoff energy depending on the particular jet and disk parameters and on the observation angle. Our unified picture of the kinematic and spectral properties of BL Lac objects in the context of the radiative deceleration scenario may also be relevant to radio-loud quasars and serves to reinforce the interpretation of these sources in terms of beamed relativistic jets.

We acknowledge useful conversations with R. Antonucci, E. Feigelson, D. Lamb, P. Madau, G. Madejski, M. Malkan, R. Mushotzky, W.-H. Sun, and M. Urry. A. K. thanks the Institute for Theoretical Physics at Santa Barbara, where part of this work was carried out, for hospitality. This research was supported in part by National Science Foundation grants AST 84-51727, AST 85-03093, and National Aeronautics and Space Administration grant NAGW-830 at Chicago, by NSF grant PHY 88-57218 at Northwestern University, and by NSF grant PHY 82-17853 (supplemented by funds from NASA) at Santa Barbara. Partial support was also provided by grants from Rockwell International Corporation and the Louis Block Fund at the University of Chicago.

REFERENCES

Abramowicz, M. A., and Piran, T. 1980, *Ap. J. (Letters)*, **241**, L7.
Angel, J. R. P., and Stockman, H. S. 1980, *Ann. Rev. Astr. Ap.*, **18**, 321.
Barr, P., Giommi, P., Pollock, A., Tagliaferri, G., Maccagni, D., and Garilli, B. 1989, in *IAU Symposium 134, Active Galactic Nuclei*, ed. J. Miller and D. Osterbrock, in press.
Barthel, P. D., Schilizzi, R. T., Miley, G. K., Preuss, E., and Hooimeyer, J. R. 1988, in *IAU Symposium 129, The Impact of VLBI on Astrophysics and Geophysics*, ed. M. J. Reid and J. M. Moran (Dordrecht: Reidel), p. 17.
Bechtold, J., Czerny, B., Elvis, M., Fabbiano, G., and Green, R. F. 1987, *Ap. J.*, **314**, 699.
Begelman, M. C., and Sikora, M. 1987, *Ap. J.*, **322**, 650.
Bignami, G. F., Fichtel, C. E., Hartman, R. C., and Thompson, D. J. 1979, *Ap. J.*, **232**, 649.
Biretta, J. A., Moore, R. L., and Cohen, M. H. 1986, *Ap. J.*, **308**, 93.
Blandford, R. D., and Königl, A. 1979, *Ap. J.*, **232**, 34.
Bregman, J. N., *et al.* 1986, *Ap. J.*, **301**, 708.
Cohen, M. H., and Unwin, S. C. 1984, in *IAU Symposium 110, VLBI and Compact Radio Sources*, ed. R. Fanti, K. Kellermann, and G. Setti (Dordrecht: Reidel), p. 95.
Cohen, M. H., Zensus, J. A., Biretta, J. A., Comoretto, G., Kaufmann, P., and Abraham, Z. 1987, *Ap. J. (Letters)*, **315**, L89.
Czerny, B., and Elvis, M. 1987, *Ap. J.*, **321**, 305.
Elvis, M. 1988, in *Proc. Rutherford-Appleton Lab Workshop on Emission Lines in AGN and Quasars*, ed. P. Gondhalekar and H. Netzer, in press.
Elvis, M., Green, R. F., Bechtold, J., Schmidt, M., Neugebauer, G., Soifer, B. T., Matthews, K., and Fabbiano, G. 1986, *Ap. J.*, **310**, 291.
Feigelson, E., *et al.* 1986, *Ap. J.*, **302**, 337.
Ghisellini, G., Maraschi, L., and Treves, A. 1985, *Astr. Ap.*, **146**, 204.
Hall, R., Ricketts, M. J., Page, C. G., and Pounds, K. A. 1981, *Space Sci. Rev.*, **30**, 47.
Königl, A. 1981, *Ap. J.*, **243**, 700.
Madau, P. 1988, *Ap. J.*, **327**, 116.
Makino, F., *et al.* 1987, *Ap. J.*, **313**, 662.
Malkan, M. A., and Moore, R. L. 1986, *Ap. J.*, **300**, 216.
Malkan, M. A., and Sargent, W. L. W. 1982, *Ap. J.*, **254**, 22.
Maraschi, L., Ghisellini, G., Tanzi, E. G., and Treves, A. 1986, *Ap. J.*, **310**, 325.
Maraschi, L., and Maccagni, D. 1988, *Mem. Soc. Astr. Italiana*, in press.
Marscher, A. P., and Gear, W. K. 1985, *Ap. J.*, **298**, 114.
Melia, F., Rappaport, S., and Joss, P. C. 1986, *Ap. J. (Letters)*, **305**, L51.
Michel, F. C. 1987, *Ap. J.*, **321**, 714.
Moore, R. L., Schmidt, G. D., and West, S. C. 1987, *Ap. J.*, **314**, 176.
Mushotzky, R. F., Boldt, E. A., Holt, S. S., Pravdo, S. H., Serlemitsos, P. J., Swank, J. H., and Rothschild, R. H. 1978, *Ap. J. (Letters)*, **226**, L65.
Mushotzky, R. F., Boldt, E. A., Holt, S. S., and Serlemitsos, P. J. 1979, *Ap. J. (Letters)*, **232**, L17.
O'Dell, S. L. 1981, *Ap. J. (Letters)*, **243**, L147.
Ohashi, T. 1989, in *BL Lac Objects: 10 Years After*, ed. L. Maraschi *et al.* (New York: Springer-Verlag), in press.

© American Astronomical Society • Provided by the NASA Astrophysics Data System

1989ApJ...340..162M

Phinney, S. 1982, *M.N.R.A.S.*, **198**, 1109.
———. 1987, in *Superluminal Radio Sources*, ed. J. A. Zensus and T. J. Pearson (Cambridge: Cambridge University Press), p. 301.
Porcas, R. W. 1987, in *Superluminal Radio Sources*, ed. J. A. Zensus and T. J. Pearson (Cambridge: Cambridge University Press), p. 12.
Readhead, A. C. S., Pearson, T. J., and Barthel, P. D. 1988, in *IAU Symposium 129, The Impact of VLBI on Astrophysics and Geophysics*, ed. M. J. Reid and J. M. Moran (Dordrecht: Reidel), p. 65.
Rees, M. J. 1981, in *IAU Symposium 94, The Origin of Cosmic Rays*, ed. G. Setti, G. Spada, and A. W. Wolfendale (Dordrecht: Reidel), p. 139.
———. 1984, in *IAU Symposium 110, VLBI and Compact Radio Sources*, ed. R. Fanti, K. Kellermann, and G. Setti (Dordrecht: Reidel), p. 207.
Shields, G. A. 1978, *Nature*, **272**, 706.
Sikora, M. 1981, *M.N.R.A.S.*, **196**, 257.
Sikora, M., and Wilson, D. B. 1981, *M.N.R.A.S.*, **197**, 529.
Smith, P. S., Balonek, T. J., Heckert, P. A., and Elston, R. 1986, *Ap. J.*, **305**, 484.
Smith, P. S., Elston, R., Berriman, G., Allen, R. G., and Balonek, T. J. 1988, *Ap. J. (Letters)*, **326**, L39.
Stocke, J. T., Liebert, J., Schmidt, G., Gioia, I. M., Maccacaro, T., Schild, R. E., Maccagni, D., and Arp, H. C. 1985, *Ap. J.*, **298**, 619.
Urry, C. M., and Mushotzky, R. F. 1982, *Ap. J.*, **253**, 38.
Urry, C. M., Mushotzky, R. F., and Holt, S. S. 1986, *Ap. J.*, **305**, 369.
Urry, C. M., Mushotzky, R. F., Kondo, Y., Hackney, K. R. H., and Hackney, R. L. 1982, *Ap. J.*, **261**, 12.
Wandel, A., and Petrosian, V. 1988, *Ap. J. (Letters)*, **329**, L11.
Wandel, A., and Urry, C. M. 1989, in *BL Lac Objects: 10 Years After*, ed. L. Maraschi *et al.* (New York: Springer-Verlag), in press.
Wilkes, B. J., and Elvis, M. 1987, *Ap. J.*, **323**, 243.
Wills, B. 1989, in *BL Lac Objects: 10 Years After*, ed. L. Maraschi *et al.* (New York: Springer-Verlag), in press.
Wolstencroft, R. D., Gilmore, G., and Williams, P. M. 1982, *M.N.R.A.S.*, **201**, 479.
Worrall, D. M. 1987, in *Superluminal Radio Sources*, ed. J. A. Zensus and T. J. Pearson (Cambridge: Cambridge University Press), p. 251.
Worrall, D. M., *et al.* 1984, *Ap. J.*, **278**, 521.

ARIEH KÖNIGL: Astronomy and Astrophysics Center, University of Chicago, 5640 South Ellis Avenue, Chicago, IL 60637

FULVIO MELIA: Department of Physics and Astronomy, Northwestern University, Evanston, IL 60208

© American Astronomical Society • Provided by the NASA Astrophysics Data System